Impact of initial and lateral open boundary conditions in a Regional Indian Ocean Model on Bay of Bengal circulation

[1]Hasibur Rahaman[*],[3]Lakshmi Kantha,[2]Matthew Harrison, [1]J V S Raju,[1]T M Balakrishna Nair,and[4]M Ravichandran

[1] Indian National Centre for Ocean Information Services,
Ministry of Earth Sciences, Hyderabad, India

[2] National Oceanic and Atmospheric Administration (NOAA)
Geophysical Fluid Dynamics Laboratory (GFDL)
Princeton, USA

[3]Department of Aerospace Engineering Sciences, University of Colorado, Boulder, USA

[4] Earth System Science Organization (ESSO), Ministry of Earth Sciences (MoES),New Delhi,India

[*] **Corresponding Author:**

Dr.Hasibur Rahaman
Indian National Centre for Ocean Information Services
Ministry of Earth Sciences, Government of India
Ocean Valley, Pragathi Nagar (BO)
Nizampet (SO)
Hyderabad - 500 090,India.
Tel: +91 40 23886052/6000
FAX: +91 40 23882910
e-mail: rahman@incois.gov.in

Abstract

This study uses three simulations (Exp-1,Exp-2 and Exp-3) from a nested basin-scale, regional, eddy-permitting Indian Ocean model forced with CORE-II inter-annual forcing, to study the impact of initial and lateral open boundary conditions on Bay of Bengal (BoB) circulation. It also evaluates the state of art reanalysis products from GODAS,SODA3 and ORAS5. Sensitivity studies using more realistic initial and lateral boundary conditions suggest that accurate initial conditions are essential for realistic simulation of the mean and the variability of temperature and salinity in the upper ocean. We also show that accurate lateral boundary conditions are also essential for realistic basin-scale simulations for the upper ocean circulation in the BoB. The model captured well the observed seasonal and inter-annual variability of salinity in the BoB. The comparison of surface currents from the regional simulations and reanalysis products with OSCAR analyses shows Exp-3 (with improved initial and lateral boudary condition) to be the closest among all three. The summer monsoon current is also most realistic in Exp-3, while the realaysis products are unable to reproduce the BoB Coastal Current structure and magnitude. This study also reports the first evidence of a coastally trapped, narrow boundary current at thermocline depth along the eastern boundary of BoB. The presence of this boundary current is noticed in all three regional solutions while most prominent in Exp-3 and nearly absent in the reanalysis products. The salt transport across 8 °N shows large seasonal and inter-annual variations during 2003-2009 in the best simulation (Exp-3),with standard deviation ranging between 77-150 psu-m^3/s upto 1000 m depth. Apart from summer and winter monsoon periods, which show the intrusion of salt into BoB from the equatorial Indian Ocean in the upper layers, we found significant salt transport at deeper depths (300-500 m) as well. The integrated inter-annual variations of the seasonal salt flux at different depths across 8 °N show presence of strong seasonal cycle in the upper layer (0-200 m). However, the seasonalty shows most prominent in the upper 50 m. The intra-seasonal variation in the deeper layers are more prominent as compared to the upper layer.

Key wards : Bay of Bengal, Nested regional ocean model, salt flux , salt transport, reanalysis

1. Introduction

Sea surface salinity (SSS) affects sea water density, which in turn impact ocean circulation and climate. Subsurface salinity (particularly in the upper ocean up to 200 m) also controls the density stratification and hence changes in circulation (Capotondi et al., 2012). Therefore, accurate simulations of SSS and subsurface salinity are essential for a better understanding of the circulation in the mixed layer and deeper ocean (Vilard and Delecluse, 1998; Durand et al., 2004). Although recent models have included freshwater forcing,they have had difficulties in reproducing the observed features of the salinity distribution, especially in the Bay of Bengal (BoB) and the southeastern Arabian Sea (SEAS) (Han et al., 2001; deBoyer Montegut et al., 2007; Durand et al.,2007; Kurian and Vinaychandran,2007). The SSS simulation errors are as large as 2-3 psu over northern BoB (Murtugudde and Busalacchi, 1999; Han et al., 2001; Han and McCreary, 2001; de Boyer Montegut et al., 2007).

Although the upper ocean heat budget studies are available with reasonable accuracy of ~ 10 W/m^2 (Bradley et al., 1995), the quantification of salt or equivalently freshwater (FW) flux is much more difficult than that of heat flux. This is mainly due to the different spatial scales of the atmospheric input functions, such as solar radiation and precipitation. Over large oceanic areas, the radiative heating of the ocean during daytime is relatively uniform. On the other hand, the FW input is closely coupled to the existence of atmospheric convection cells, which are relatively small in size and irregularly distributed in space, and have no diurnal signal like the heat flux.

Salinity in the North Indian Ocean (NIO) is strongly influenced by river inflows in BoB, the influx of low salinity Pacific water throughflow in the Indonesian Archipelogo, and the inflow of saltier water from the Persian Gulf and Red Sea. BoB also receives a large quantity of FW from rainfall during the summer monsoon season (June - September). In contrast, excessive evaporation and uneven distribution of precipitation and river discharge make the Arabian Sea (AS) saltier than BoB. Under steady state conditions, FW from BoB should be exported to AS, and salt water from AS to BoB. The inter-ocean exchange and transport of FW have been studied in detail by Gordon (2001) and Wijffels (2001). Many previous studies have shown the locations of inter-basin exchange of FW and salt between BoB and AS

(Nyadjro et al., 2010, 2011; Jensen et al., 2001,2003,2016; Vinayachandran et al., 1999, 2013; Sanchez-Frankset al., 2019; Sheehan at al., 2020). However, the details on the magnitude of the freshwater transport and its seasonal and inter-annual variability are not as well known. Recent HYCOM model simulations (Jensen et al., 2016) show a large persistent flow of high salinity water from the equatorial Indian Ocean into BoB during the northeast monsoon,but weaker than during the southwest monsoon. Jain et al.,(2017) have shown that three high-salinity water masses, i.e., Arabian Sea high-salinity Water (ASHSW), Persian Gulf Water (PGW), and Red Sea Water (RSW) are advected into BoB by the Summer Monsoon Current (SMC), which is a deep current extending to a depth of about 1000 m (Vinayachandran et al., 1999,2013; Sanchez-Franks et al., 2019; Sheehan et al., 2020). Sengupta et al. (2006) have shown that FW from BoB river runoff reaches remote regions of AS. It also crosses the equator in the eastern BoB and subsequently flows across the southern tropical Indian Ocean. Several studies also show that low salinity surface water from northern BoB flows down the east coast of India in October–December through the East India Coastal Current (EICC, Shetye et al., 1996; Prasanna Kumar et al., 2004; Gopalakrishna et al., 2005; Rao and Sivakumar, 2003). Modelling experiments show BoB water enters the tropical Equatorial Indian Ocean (EIO) to the east and south in the second half of the year, crossing the equator mainly in the east (Jensen, 2003; Miyama et al., 2003). Using Reanalysis data, Nyadjro et al. (2013) describe near-surface horizontal salt flux in the Indian Ocean during 1960–2008. Kantha et al. (2008) studied NIO circulation and its variability, as well as, meridional heat fluxes, using a 0.5-degree resolution numerical hindcast model, assimilating altimetric and SST data for the years 1993 to 2004. However, they did not investigate salt fluxes in NIO, because at the study time remotely-sensed SSS was not yet available for assimilation into the model. The readers are referred to this paper for a nice summary of NIO circulation and relevant issues.

As explained in the previous section, previous studies have reported that the inter-basin exchange of subsurface salt transport to and from BoB to SEAS and EIO and vice versa occurs. However, despite the extensive studies of salt exchange between the two basins, BoB and AS, on its mean state, its seasonal and inter-annual variability and their frequencies are not very well known, particularly in the deep ocean. One of the reasons for this is the lack of realistic simulation of meridional currents in BoB (see Kantha et al., 2008). In this study, to

overcome this deficiency, we use simulations from a nested Indian Ocean model developed by Rahaman et al (2014),which show realistic boundary current and FW transport in BoB. We compare the model simulated currents and salinity with observations.

Modeling the oceanic circulation is made difficult by the wide range of spatial scales from the Rossby radius of deformation (10 to 50 km) to the basin scales. Global ocean general circulation models (OGCM) require high spatial resolution to represent geostrophic eddies, narrow boundary currents, and flows through passages. Available computer resources often limit the development of high resolution global models to represent all these physical phenomena. Alternative option is to develop a basin scale, high resolution regional models to meet this challenge with a reasonable amount of computer resource consumption (Griffies 2009; Treguier et al., 2001). However, to work with a basin scale, regional model, open boundary conditions (OBCs) must be applied at the lateral open boundaries, which permit fluxes of mass, heat, momentum into and out of the model domainfrom an outer larger scale model (e.g., GOCM),often called a parent model. Open boundaries, which naturally occur in a regional model, are often difficult to handle due to an inherently, mathematically ill-posed problem at the boundary. The numerical solution near a boundary is always a superposition of outgoing and incoming waves (as well as scalar and momentum fluxes), which cannot be separated and there is no universally perfect scheme for open boundary conditions (Stevens, 1991; Griffies, 2009).

Two types of lateral open boundary conditions are used in regional ocean models, which are generally referred to as "active" or "passive". In the passive type, the OBCs are determined solely from model solution within the computational domain. On the other hand, in an "active" type, data are prescribed from an external source (e.g., a larger scale model) to force the interior solution. Since the behavior of the model interior is rarely consistent with data prescribed at the boundary, the model may become prone to errors due to under-specification (not enough information describing external processes is provided) or over-specification (OBC information is incompatible with interior state). Reader may refer Marchesiello et al. (2001) for a thorough discussion of the active versus passive boundaries, and over vs. under-specification of data. When the interior model solutions are determined only by the information imposed at the boundaries from outer models,and interior (child) solutions do not affect the exterior (parent) solutions, it is called one-way nesting. On the

other hand, if the interior solutions also affect the exterior solutions across the boundaries between the two, it is called two-way nesting. One way nested models have been developed with great success, for instance, in the California Current region (Penven et al., 2006) and Benguela Upwelling area off the coast of Namibia (Hertzfel et al., 2011). Recently, two-way nesting using finite difference models has gained popularity in refining solution in the regionaldomain (e.g., Cailleau et al., 2008; Jouanno et al., 2008; Barth et al., 2005; Sheng et al., 2005). For a detailed review of two-way nesting, readers are referred to Debreu and Blayo (2008).

One-way nested approach has been adopted in the present study and OBCs are prescribed from a global model solutions. Flather radiation condition (Flather, 1976) has been used for the depth averaged normal velocity at the eastern and southern boundary of the Indian Ocean model. The flow relaxation scheme of Martinsen and Engedahl (1987) has been used for the temperature and salinity at the boundary. The details of OBCs and other model configurations can be found in Rahaman et al. (2014).

For the earth system model's or climate model's simulation accuracy, in terms of hindcast or predictions on different time scales, accurate initiliziation of ocean plays a major role. The skill of climate system forecasts at the sub-seasonal to seasonal (S2S), seasonal to inter-annual (S2I) and seasonal to decadal (S2D) scales depends on the oceanic initial conditions fed into the models, in particular, information on the ocean's upper thermal and salinity structure (Alves et al., 2004; Balmaseda et al., 2009,2013,2015; Meehl et al., 2021). Halliwell et al. (2011) have demonstrated that accurate ocean model initialization with respect to the upper-ocean temperature and salinity (density) profiles, along with the correct location of ocean currents and eddies, is the most important factor influencing the accuracy of SST forecast by an ocean model over the northwest Caribbean Sea and Gulf of Mexico. Recently Zhu et al. (2019) have shown that the initial condition errors occurring in the Indian Ocean temperature cause "Spring Predictability Barrier" for El Niño in the Pacific Ocean. However, to our knowledge no such studies showing the impact of ocean initial condition on Indian Ocean simulations or forecasts from a forced ocean model are available. Hence, in this study, we demonstrate the impact of ocean initial conditions on BoB simulation.

In recent times, global reanalyses are available at 1/4 degree resolution based on NEMO from ECMWF,CMCC etc. and at 1/12 degree resolution from HYCOM consortium and GLORYS12 reanalysis data set produced by Mercator Ocean International forecasting center (Verezemskaya et al., 2021; Lellouche et al., 2018).

However, assimilation into global models often degrades the circulation features (Mercator Ocean, 2018). In most of these global models ocean grid generation the bathymetry is often smoothed to avoid numerical instability. As a result, topography can be too deep near the coast and narrow channel can be deeper and wider than they should. For example the bathymetry used in the global model configuration in GODAS opened the Palk Strait and made it deeper, which is not realistic (Figure 1b). The costal regions also became deeper. Hence, the costal circulation patterns are not realistically represented in global models. In this study,we used the modified bathymetry from Sindhu et al. (2007) in the regional model. Most of the ocean model configurations are based on smoothed bathymetric data sets like ETOPO5 and ETOPO2. Sindhu et al. (2007) have shown that these bathymetries are inaccurate in depths of less than 200 m along the coast of India. They modified ETOPO bathymetry along the Indian Ocean coast by digitizing the depth contours and sounding depths less than 200 m from the hydrographic charts published by the National Hydrographic Office, India. In the present study,we used this modified bathymetry (Figure 1a) for the regional ocean model configuration. The differences near the Indian coast in regional and global models can be seen in Figures 1a,b. More accurate shallow coastal bathymetry leads to significantly improved and realistic coastal circulation compared to that from global model simulations (see the discussions in Section 3.2).

Near the coast,data are often sparse, particularly in a basin like BoB. Due to lack of observations, often few data are assmilated in a global model. Hence, configuration of a basin scale model with realistic bathymetry is essential. Recently,Rahaman et al. (2020) have shown how the circulation patterns,even in the open ocean, change in the Indian Ocean with different bathymetries used in a suite of 16 global models. We show here the improved circulation features in the regional models as compared to the state-of the-art reanalysis data from GODAS, SODA3 and ORAS5.

We also show the subsurface salt transport and its interannual variability from BoB to EIO and vice versa, along with the seasonal and inter-annual variability of salt flux. Section 2

describes the data sets used in this study and the model configuration. Model results and discussion are presented in Section3 and finally,summary and conclusions are provided in Secion 4.

2. Model and data

We have adopted a nested multi-model approach using MOM4p0d/MOM4p1global Ocean General Circulation Model (OGCM) and a regional model of the Indian Ocean (Rahaman et al., 2014) based on MOM4p1. The regional model domain covers the Indian Ocean between 30 °S and 30 °N, and 30 °E and 120 °E, with a uniform horizontal resolution of 0.25°. There are 50 levels in the vertical with 1 m resolution in the upper 10 m. The regional model is forced by Coordinated Ocean Reference Experiments (CORE-II) inter-annual data. The global model uses annual river runoff, but the regional model uses seasonal river runoff (Dia and Trenberth, 2002) distributed over several grid points near the river mouths into the upper 5 m of the water column. More realistic simulation of north BoB salinity stratification can be attributed to this refined resolution(~ 1 meter near the surface), more realistic topography, and the inclusion of seasonal river runoff (Rahaman et al., 2014). The circulation and the wave propagation in the BoB are more realistic in these model simulations when compared with observations (Rahaman et al., 2014). A detailed description of the model configuration and validation can be found in Rahaman et al. (2014).

All global OGCMs suffer from excessive thermocline diffusion and hence a deeper theromocline when compared to observations (Rahaman et al., 2020). This was also the case in the regional model,which uses initial conditions from MOM4p1 global OGCM (Rahaman et al., 2014). The problem of the diffuse thermocline is rectified in a data assimilative global model (Ravichandran et al. 2013; Behringer et al., 2007; Rahaman et al. 2016,2018). The National Centers for Environmental Prediction *(*NCEP) and the Indian National Centre for Ocean Information Services (INCOIS) produce global ocean analyses/reanalysis based on the Global Ocean Data Assimilation System (GODAS). This system uses a state-of-the-art ocean general circulation model called modular ocean model (MOM4p0d) and the 3D-Variational (3DVar) data assimilation technique to assimilate observed temperature and salinity profiles from in-situ observations (Argo, Buoy,XBT, etc). We used INCOIS-GODAS reanalysis for the initial and lateral boundary conditions in the Indian Ocean Model for this study. We used

245 the same reanalysis products based on MOM4p0d,as in Ravichandran et al. (2013) and
246 Rahaman et al. (2016).
247 In this study we demonstrate how the upper ocean simulations improved in a regional
248 model by initializing with reanalysis data. Also,we show that the improved lateral boundary
249 conditions also affect the BoB simulation.We performed three Indian Ocean regional model
250 simulations: (1) Exp-1: Using initial and lateral boundary conditions from 1^{o} MOM4p1
251 global model (Rahaman et al., 2014); (2) Exp-2: Using initial conditions for 2003 from
252 INCOIS-GODAS reanalysis (Ravichandran et al. 2013,Rahaman et al. 2016), but lateral
253 boundary conditions from 1^{o} MOM4p1 global model (Rahaman et al. 2014); (3) Exp-3:
254 Using both initial and lateral boundary conditions from INCOIS-GODAS reanalysis
255 (Ravichandran et al., 2013;Rahaman et al., 2016). The details of the boundary conditions
256 applied can be found in Rahaman et al. (2014). In Exp-1 we used both initial and boundary
257 condition from MOM4p1 and in Exp-2, we just changed the initial condition of MOM4p1
258 with GODAS reanalysis, but used same lateral boundary condition of Exp-1, so that
259 comparison of Exp-1 and Exp-2 will give the impact of initial conditions. In Exp3 we also
260 replaced the lateral boundary condition with GODAS reanalysis. Hence, comparison of Exp-
261 2 and Exp-3 gives the impact of lateral boundary conditions.
262
263 Temperature and salinity from ARGO profiling floats were used to ascertain the impact of initial
264 and boundary conditions on temperature and salinity observed in the regional model. The observed,
265 gridded subsurface temperature and salinity data from Coriolis Ocean Dataset for Reanalysis
266 (CORA) were also used to determine the seasonal and inter-annual variability of temperature and
267 salinity, and geostrophic currents. The geostrophic currents for both observations and model
268 simulations were computed using dynamic height. The comparions were then made with the
269 100-500 m depth-average current. We used the latest version CORA5.2 (Cabanes et al.,
270 2013; Szekely et al., 2019) for this study. The CORA dataset is distributed by Copernicus
271 Marine and Environment Service (https://resources.marine.copernicus.eu/products). This
272 dataset used many types of in-situ temperature and salinity measurements with a maximal
273 sampling, including high frequency profilers (ARGO, CTD), surface and sub-surface time
274 series (Thermosalinographs and surface drifters). Most of these CORA profiles are collected by
275 the Coriolis data center. The CORA 5.2 dataset is an incremental version of the previous

CORA datasets, covering the period 1950 to the present.We also used AVISO monthly gridded sea level anomaly data to show the presence of eddies in BoB.

To evaluate the circulation features of regional model simulations in the BoB, we used the most recent version of 1/4 degree Ocean Surface Currents Analyses Real-time (OSCAR) surface currents (Bonjean and Lagerloef, 2002). We also used 1/4 degree Surface Currents from Diagnostic model (SCUD) based on a simple diagnostic model, which combines AVISO maps of sea level anomalies and QuikSCAT surface winds and is tuned to best reproduce trajectories of real drifters, drogued at 15 m depth (Maximenko and Hafner, 2010).

Simple Ocean Data Assimilation ocean/sea ice reanalysis (SODA) is the most widely used reanalysis data since late 20th century (Carton et al. 2000a,b,2008). Recent SODA Version 3 release now uses GFDL MOM5/SIS numerics at finer 1/4°x1/4°x50 level resolution (28 km at the Equator down to <10 km at polar latitudes), similar to the ocean component of the GFDL CM2.5 coupled climate model, and includes an active sea ice component. The Optimal Interpolation filter has also been augmented (relative to previous releases) with bias correction to reduce bias in estimates of long term trends of variables such as heat content (Carton et al 2018). We used SODA3 to compare the BoB circulation features with IOM simulations (Exp-1,-2,-3). We also included 1^{o}x1^{o} resolution ORAS5 realysis products produced by ECMWF usingthe estimates of the state of the global ocean fromthe operational system OCEAN5 (Zhu et al. 2017,2019).

The general expression for the transport or *flux* (F) of a property is the integral of the property (P) times velocity (v) over the area (dA). The area is a cross section, i.e. the width of the current times its depth.

$F = \int P*v \, dA$

Here in this study, we used P=S, where S is the salinity in psu.

Finally, a we show the schematic of major currents along the Indian coast during summer and winter seasons in Figure 1c (adapted from Bharti et al., 2021).

3. Results and Discussion

3.1 Impact of initial and boundary condition on temperature and salinity

306 The temperature and salinity determine the density and hence the ocean structureand
307 dynamics (Cooper, 1988; Murtugudde and Busalacchi, 1999). Murtugudde and Busalacchi
308 (1999) have shown that salinity plays an important role in the model dynamics and
309 theromodynamics. Hence, a realistic model simulated-circulation requires realistic
310 simulations of ocean mean temperature and salinity and their variability. As discussed in the
311 previous section,three different experiments are performed to determine the impact of initial
312 and boundary conditions, using regional model solutions. To see how well the model
313 simulates temperature and salinity with respect to observations, we have used individual
314 Argo temperature and salinity profiles,as well as gridded data. Figure 2a shows the upper
315 ocean mean (2006-2009) collocated and concurrent temperature from the three different
316 experiments with Argo profiling float observations. The trajectory of the Argo float used for
317 the co-location can be found in the subset of each panel. The magenta colour profile is from
318 Exp-1. The cyan-colored profile shows the temperature from Exp-2, which used warm start
319 (1 January 2003) with initial conditions from GODAS reanalysis and lateral boundary
320 conditions from the inter-annual global model solutions (1992-2009) based on MOM4p1
321 (same lateral bondary condition of Exp-1). It can be seen that the large thermocline bias in
322 the Exp-1(magenta lines) is drastically reduced and the profiles are closer to Argo
323 observations in Exp-2 (cyan line). It is worth mentioning that for Exp-2, we used GODAS
324 reanlysis data to initialize, whereas Exp-1 used solutions from a non-data-assimilative global
325 model (see Rahaman et al., 2014 for details). This demonstrates that better initial conditions
326 have improved model simulations. Furthermore, when lateral open boundary conditions from
327 GODAS reanalysis are also used (Exp-3), the simulated temperature (blue line) almost
328 matches the Argo observation (black line). It is worth mentioning that even 3 years after
329 initialization, the theromocline is well maintained in the model and it persists even until the
330 7th year. The 0-500 m depth mean bias in Exp-1 is 2.1 °C, which is reduced to 1.1 °C in Exp-
331 2 and only 0.41 °C in Exp-3.
332 Figure 2b shows the monthly STD in the upper ocean (0-500 m). Similar results can be
333 seen in the standard deviation (SD) of temperature as well. The Argo observed variability
334 (black line) in terms of SD is most accurately captured by Exp-3. The highest observed SD
335 values of 2.3 °C at 90 m depth is almost reproduced in Exp-3 (2.0 °C, blue line). The 70-110
336 m depth-averaged STD in Argo observation is 2.2 °C, while it is 1.78 °C,1.79 °C and 1.92° C

for Exp-1, Exp-2 and Exp-3, respectively. However, the RMSD value increased slightly in Exp-3(0.85 °C), as compared to Exp-2 (0.81 °C) and Exp-1(0.78 °C). This slight increase may be due to the bias present in 2006 in the original GODAS reanalysis data.

The co-located and concurrent mean salinity from the three experiments in the upper ocean are shown in Figure 2c. The observation (black line) shows salinity increases gradually in the upper ocean until a depth of 150 m and afterward, it is almost constant. Exp-1(magenta) shows a slight underestimation of salinity in the upper layers (150 m) and a slight overestimation in the deeper layers (deeper than 150 m) compared to observations. However, although experiments with GODAS initial as well as boundary conditions (Exp-2 and Exp-3) show somewhat lower salinity values in the upper ocean (to 150 m), they follow the observed Argo mean values quite well below 150 m. The freshening in the upper 100 m may be due to higher vertical resolution of the model. In the upper 100 m, the model has 23 levels , starting from 0.5 m up to 20 m the resolution is 1-3 m; thereafter it slowly increases to 10 m at 103 m depth. In contrast, the Argo profiling float has uniform resolution of 5 m in 0-100 m depth and 10 m between 100-500 m. All the three experiments miss some of the structure in the upper 75 m for temperature and salinity when compared with Argo observation. This could also be due to the refined vertical resultion in the model as compared to Argo observation. The mean bias in Exp-1 is 0.01 psu which is slightly saltier when compared to Argo observation. However, with GODAS initial and boundary conditions, it becomes slightly fresh with mean bias of -0.11 psu and -0.09 psu in Exp-2 and Exp-3, respectively. Salinity bias in Exp-1 in the thermocline region (150-500 m depth) is ~ 0.08 psu, which is significant for the spiciness variability. The same for Exp-2 and-3 is ~ -0.01 psu. The spiciness variability in the thermocline is believed to be an important subsurface ocean process affecting sea surface temperature (SST) and climate variability over the tropical Indian Ocean (Li and Wang 2015).

The observed salinity variability represented by the STD is also picked up by all three experiments and the solutions with GODAS initial and boundary conditions closely follow the observed variability (Fig.2d). The Argo STD is 0.07 psu, Exp-2 and-3 show 0.09 psu, which is the closest to the observed value in contrast to Exp-1,which shows slightly higher STD value of 0.11 psu. The RMSD valueis also lowest in Exp-3 (0.09 psu), compared to Exp-2 (0.1 psu) and Exp-1 (0.12 psu). This is the first co-located and concurrent salinity

368 comparison of the impact of initial and lateral boundary conditions in a regional model
369 simulations of BoB. Wakelin et al. (2009) have shown the impact of initial and open
370 boundary conditions for a northeast Atlantic implementation of the Proudman Oceanographic
371 Laboratory Coastal Ocean Model System (POLCOMS) from WOA observations and two
372 large scale operational ocean models (Forecasting Ocean Assimilation Model (FOAM), UK
373 Met. Office and the Navy Coastal Ocean Model (NCOM), US Naval Research Laboratory).
374 They show that in the shelf region,after 15 months of model integration, the effect ofthe
375 temperature and salinity initial conditions was negligible, and the model dynamics and
376 surface forcing play a dominant role. However, in the deep regions, NCOM boundary
377 conditions resulted in smaller RMS errors in the SST simulations than the FOAM boundary
378 conditions. These results further confirm the finding in BoB.
379 In order to see the seasonal behavior of the model solutions, we show the comparison of
380 seasonal average co-located and concurrent upper ocean temperature from the three
381 experiments with Argo observation during 2007-2008 (Fig. 3). The trajectory of the Argo
382 used for the co-location can be found in Figure 3b. On seasonal scale,it also shows similar
383 results for the mean (Fig. 3a). In the mean plot, the Exp-3 closely follows the Argo
384 observation,but in 2007-08 there is a slight warm bias in the thermocline in Exp-3 in summer
385 (July-Aug) and fall (Sept-Oct). It should however be noted that the trajectory of Argo float
386 was confined to the southwest BoB. In order to see whether the same results hold for the
387 entire basin as well, we compared the subsurface tempertaure from ORCA5.2 gridded
388 observations (see Figure 5-7).
389 Seasonal comparison of subsurface salinity along the Argo trajectory in 2007-2008 are
390 shown in Figure 4. In contrast to temperature, which shows that the impact of initial and
391 boundary conditions is uniform in different seasons, the salinity comparison shows the
392 impact is most prominent during summer and fall. The observed salinity profile is well
393 reproduced in Exp-2 and Exp-3 during summer and fall, except in the upper ~100 m in which
394 the model shows fresher values compared to Argo profiling float observation. This could be
395 due to the higher vertical resolution in model than in Argo observation, same as for the
396 temperture. During winter and spring, the salinity simulation shows degradation in the
397 thermocline region in Exp-2 and Exp-3 when compared to Exp-1. The degradation in winter-
398 spring vs summer-fall could be due to the deficiencies in the forcing fields or could be

related to the model itself and its inability to capture physical processes in Winter-Spring vs Summer-Fall for 2007-2008. However, below the thermocline, salinity simulations in Exp-2 and Exp-3 are almost reproduced in all seasons.

Seasonal monsoon rain and river runoff create shallow pools of freshwater in the north BoB in summer (Gopalakrishna et al., 2002; Vinayachandran and Kurian 2007) and autumn. In-situ observations in the north BoB (Sengupta et al., 2006; Shetye et al., 1996) often show an intense, shallow halocline at 5–20 m in depth. Our model simulations reproduce this observed strong salinity stratification inthe upper layers of the northern BoB. However, the Argo profiling float is unable to capture this due to its coarse vertical resolution (5 m between 5-100 m ;10 m between 100-500 m and 25 m between 500-2000 m). Model reproduced the salinity profiles well,when compared with high vertical resolution,specially operated individual Argo float data as well as CTD observation (figure not shown).

The comparions above were made with a single profile data. In order to see the robustness of this comparison, we used the latest gridded subsurface temperature and salinity observations from CORA5.2. Figure 5 shows comparisons of model-simulated mean temperature and salinity from the three experiments to CORA5.2 observations in the northern BoB. Results in the northern BoB are very much similar to those in Figure 2, but the impact of initial and boundary conditions is more prominent in the temperature fields than in salinity (Figure 5a,b). GODAS assimilates actual salinity and temperature profiles. We used the initial condition from 2003. In 2003,the number of salinity profiles over the northern BoB are fewer than the number of temperature profiles that goes into the GODAS analysis. Hence, the simulated reanalysis temperature fields are more accurate than the salinity fields. This is reflected in regional model solutions also.

From Figure 5, it is difficult to judge whether the large warm bias in Exp-1 in 200-800 m depth is uniform or has interannual variation. Therefore, we present the depth vs time plots of the difference between the three model simulations and the observed gridded temperature showing interannual variations over northern BoB in Figure 6. It can be seen that large warm bias of ~3 °C in the therocline in Exp-1 is uniform throught the entire time period. This bias is reduced to ~1 °C in Exp-2 and further to only ~0.5 °C in Exp-3. In all three experiments, the upper ocean (0-100m) is cooler by ~ 0.5-1 °C. This cooler bias could be due to the biases in the CORE-II forcing fields used or in accurate mixed layer mixing scheme (Rahaman and

Ravichandran, 2013; Rahaman et al., 2020). All three experiments show fresher waters in the upper ocean (0-200 m)(Figure 7). The subsurface bias is within +/- 0.1 psu in all these experiments (Figure 7). As explained above, the improvement in salinity is not as significant as temperature in Exp-2 and 3. This could again may be due to the salinity bias in the original GODAS reanalysis data itself or forcing fields or deficiencies in model physics.

It is clear that the salinity bias is the lowest in Exp-3. Therefore, we look further at the salinity bias in Exp-3 in a smaller region. Figure 8 shows the depth vs. time plots of model minus observation, averaged over 80-92 °E and in two sections, one over central BoB (12-16 °N :Figure 8a) and another over southern BoB (6-10 °N :Figure 8b) (see Figure 1a for the geographical location of these regions). The upper 40 m shows that the model overestimates salinity by 0.4-0.6 psu in central BoB (Figure 8a). Below this layer model salinity is fresher by 0.2 psu w.r.t. gridded observations. In the southern BoB, the model shows freshening compared to observations. Sharma et al. (2010) have reported model simulated SSS with root mean square error (RMSE) of ~ 0.4 psu when compared with RAMA (Research Moored Array for African-Asian-Australian Monsoon Analysis and Prediction) buoy observations. However, their results are from the Equatorial Indian Ocean buoy. This low bias of ~ 0.2-0.6 psu at seasonal and inter-annual time scales has not been reported in any of the earlier model simulations in the BoB (deBoyer et al. 2007; Sharma et al., 2010; Jensen et al., 2016).

3.2 Impact of initial and boundary conditions on Bay of Bengal circulation in the regional model and reanalysis data

As explained in the introduction, the circulation pattern can change with bathymetry patricularly in the coastal region. In this section, we present BoB circulation features in our simulations and how they differ from state-of-the-art reanalysis data. We compared the spatial current patterns from regional model simulations Exp-1,Exp-2 and Exp-3 and from GODAS,SODA3 and ORAS5 reanalysis data,with the OSCAR and SCUD analysis data. We also compared model simulated geostrophic currents computed with 100- 500 m temperature and salinity fields with that of gridded observations. Figure 9 shows the time series of meridional currents averaged over central and southern BoB. It can be seen that the model was able to capture the meridional component of geostrophic current quite well (Fig.9a,b). The hydrographic observations show the east-west salinity gradient during winter time along

461 the eastand west coast of India (Shetye et al., 1991a,1996). The model captured this east-west
462 gradient also with good accuracy (not shown).
463 The OSCAR analysis is widely used to evaluate the spatial variation of suface currents
464 from model simulations. It is considered independent observations since as per our
465 knowledge no reanalysis products with assimilation of current are avalable. We used OSCAR
466 analysis (Bonjean and Lagerloef, 2002) to evaluate how the modeled currents compared with
467 observations in the regional models (Exp-1,Exp-2 and Exp-3) and also from recent state-of-
468 the-art reanalysis products from GODAS,SODA3 and ORAS5. We also used another
469 observation SCUD, which is produced from the combination of geostrophic and Ekman
470 currents derived from SLA and QuikScat wind observation (Maximenko and Hafner, 2010)
471 (see Sec2 for more details about the data sets). Figure 10 shows 2003-2009 mean upper
472 ocean currents (0-30 m) from the three experiments and OSCAR, SCUD analysis and three
473 reanalysis products i.e., GODAS,SODA3 and ORAS5. The circulation features in both
474 observed data show similar variations along the east coast of India and southern tip of Sri
475 Lanka. But theydiffer in circulation features along the west coast of India and eastern BoB.
476 The EICC structure is very prominent even in the seven year (2003-2009) mean in
477 observations (Figure 10a,b).The regional models accurately simulate the width of the EICC
478 structure as seen in the observation. The model currents are in good agreement with the
479 OSCAR analysis. They are also in good agreement with previously reported model
480 simulations (Jensen, 1991; Vinaychandran and Yamagata 1998; Vinachandran et al., 2005).
481 However, the global reanalysis products are unable to reproduce the narrow EICC structure
482 (Figure 10d,f,h). In Exp-1, the EICC shows weak circulation.With improved initilization in
483 Exp-2, its magnitude is enhanced,and further with both updated initilization and boundary
484 condition in Exp-3, the EICC structure is close to observations (Figure 10a,b,c,e and g). As
485 explained in the introduction section, without realistic bathymetry represenation in a global
486 model, the coastal circulation may not be realistic. This can be seen in Figure 10d for
487 GODAS reanalysis product, which shows strong flow through Palk Straight, whereas in
488 reality there is no flow (Rao et al. 2011). Figure 11 shows the surface current (0-30 m)
489 monthly varibility in terms of STD from OSCAR and SCUD analyses, all regional model
490 simulations and reanalysis products. The two analysis-based observations shows large
491 variability to the east of Sri Lanka and over the southern top of India. If we take OSCAR as

the reference, the regional simulations with updated initial and boundary condition reproduced the observed spatial variability most closeast to the obsetrved variability among all regional simulations (Figure 11a,g). However, all the regional simulations underestimates the magnitude. Among the realaysis products, GODAS is closer to obsservation but it overestimates the observed STD over the southern tip of India.

Accurate seasonal varition of ocean currents are crucial to determining salt balance in BoB (Nyadjro et al., 2010, 2011; Jensen et al., 2001,2003,2016; Vinayachandran et al., 1999,2013,2018). On the east coast of India during inter-monsson period,a strong costal current named EICC flows towards the pole (equator) during February-May (October-December) and peaks in April (November) (Shetye et al., 1993,1996). Many observational and modeling studies have reported the transport of low salinity north BoB water by EICC into the eastern Arabian Sea in October and November. (e.g. Han et al., 2001). This equatorward (poleward) EICC during November (April) and monsoon currents in the open ocean are responsible for maintaining the salinity balance in the BoB. As such, accurate representation of EICC is crucial for the salt balance in the BoB. Global models are unable to capture this strong, narrow EICC. Hence, we evalauted the surface circulations of regional model simulations and reanalysis products with analysis based observations (OSCAR and SUCD). In January, two anti-cyclonic circulations, one over northwest BoB and another over southeast BoB prevail within a basin-wide anti-cyclonic gyre. In the southwestern BoB, along the east coast of Sri Lanka and the southern part of the east coast of India, one can see the presence of strong, narrow equatorward currents. Just east of this equatorward current, a strong, broad poleward current is present as part of the basin-wide cyclonic gyre. This observed circulation pattern is very well reproduced by the regional model simulations (figure not shown). Figure 12 shows the upper ocean (0 to 30 m) mean (2003-2009) current for April,representative of spring season from the regional model simulation i.e.,Exp-1,-2 and -3, and GODAS,SODA3 and ORAS5 reanalysis products. Obsevation shows that at ~ 8 °N, the westward flowing North East Monsoon (NEM) current bifurcates into two branches when it reaches Sri Lankan coast. The northern branch flows as a strong narrow EICC along the east coast of the India flowing from 8 °N to 16 °N when it leaves the coast. The other branch flows towards west around the tip of Sri Lanka. This detachment from coast of EICC has been reported by Babu et al. (2003). The observed EICC structiure is well reproduced in

regional model simulations as compared to the reanalysis products. In April, the BoB circulation pattern shows a single weak gyre with strong EICC as part of it (Shetye et al., 1996). This gyre structure is well reproduced in all the simulations. The northeastward current at 4 °N along 86-96 °E splits into two at 6 °N which is well reproduced in regional simulations and GODAS reanalysis but is weak in SODA3.This spliting absent in ORAS5. GODAS reanlaysis shows unrealistic strong flow throgh Palk Strait north of Sri Lanka,whereas it is realistic in all other simulations. It is worth mentioning that in many earlier modelling studies, the Malacca Strait was closed. However, in reality,the Strait,the world's busiest ship route,with a 25 m deep narrow channel has considerable flow through it (Daryabor et al., 2016). In the present regional model set up, this channel is kept open with realistic bathymetry(see Figure 1a). This can be seen in the flow coming from the East China Sea through the Malacca Strait (Figure 12).

Figure 13 shows the upper ocean (0-30 m)mean current in July. The spatial structure resembles the monsoon current driven by the southwest monsoon wind. Both observations show the presence of strong Southwest Monsoon Current (SMC),which flows eastward below south of India, turns around Sri Lanka and flows northeastward into the BoB. All three regional model simulations and reanalysis products were able to capture this SMC. Over the east of Sri Lanka the magnitude is closest to observation in Exp-3 , however south of Sri Lanka SMC magnitude is better represented in Exp-1 as compared to other experiments. The improvemnet of magnitude from Exp-1 to Exp-3 clearly signifies that the improved initial and lateral open bounadary conditions improve the SMC simulation. Among the reanalysis products, GODAS overestimates the current and its direction also differs,compared to both the observations as well as other simulations. SODA3 shows the weakest SMC among all. Observation shows that at the height of summer monsoon, there is a western boundary confluence near 10 °N with the EICC flowing northward to the north of 10 °N and southward south of it (Vinayachandran et al.,1999; Eigeneheer and Quadfasel,2000). This bifurcation of current near to the coast at about 10 °N is most realistically present in Exp-3 (Figure 13a,b,e). All the reanalysis products show weaker southward component as compared to observations (Figure 13a,b,d,f,h). However, in the regional model simulations with improved initial and lateral bounadry conditions (Exp-3) it is realistic compared to observations (Figure 13a,e,g). The strong WICC flowing equatorward along the west coast of

554 India, driven by strong summer monsoon wind, is prominently seen in both observations
555 (Figure 13a,b) (Cutler and Swallow, 1984; Shetye and Shenoi,1988); however they differ in
556 magnitude. All the simulations are able to reproduce this WICC, but differ in magnitude.
557 Exp-3 among the regional models and ORAS5 among the reanalysis products are closest to
558 observations. The circulation in the western BoB and in the Andaman Sea differs
559 significantly in the regional model simulations and reanalysis products. Over this region, the
560 two observations shows similar circulation pattern with OSCAR weaker compared to SCUD.
561 The reanalysis products somewhat match the OSCAR observation. The accurate bathymetry
562 representation leads to realistic coastal circulation in the regional simulations. The strong
563 southeastward current at the tip of northern Anadaman Island is present only in the regional
564 model simulations. This also may be due to topograpy induced enhancement of current
565 (Gopalakrishnan and Cornuelle, 2019).
566 All three regional models show broader southwestward currents along 90-98 °E towards
567 the equator; observations also show this but with much narrower width. Reanalysis products
568 are close to observations. The southern Bay reflects two different paths, narrow strong
569 northward current in the western part and a relatively weak broader southward current in the
570 eastern part.
571 Figure 14 shows the mean surface currents over the BoB in November. A narrow current
572 flows from north BoB along the east coast of India and after turning around Sri Lanka, it
573 reaches till Gujarat Coast with a slightly broader band along the west coast of India. It is
574 worth mentioning that the Palk Strait is closed in Exp 1-3. This narrow modeled current
575 along the coast is quite realistic in regional models (Exp-1-3) (Figure 14a,c,e,g) when
576 compared with OSCAR observations. As expected, the reanalysis products are unable to
577 reproduce the structure and magnitude of equatorward EICC. Wijesekera et al. (2015) have
578 shown that the tracks of eight drifters deployed east of Sri Lanka and southern BoB between
579 24 October and 23 December 2013 show a similar narrow current (see their Figure 4). Along
580 85-90 °E,a strong poleward current can be seen, which extends to northern BoB.
581 The thermocline temperature and salinity shows large variability in 50 -200 m depth
582 (Fig.2b,d) and this variability must be reflected in the circulation near thermocline region.
583 Also the the temperature and salinity gradient is more prominent at 50-200 m depth range
584 (Fig.2a,c). Hence in order to see the seasonal spatial variation of thermocline current we

choose 50 - 200 m depth average current. We have shown the mean thermocline current for April in Figure 15. The circulation pattern in the thermocline resembles the surface circulation features seen in Figure 12, but is much weaker. The prominent cyclonic and anti-cyclonic eddy structures are seen in the sea level data (Figure 15 b). The geostrophic current computed with CORA5.2 temperature and salinity data is shown in Figure 15a. Presence of basin wide prominant anti-cyclonic gyre can be seen, which supports earlier findings (Varkey et al., 1996). In the spring, the anti-cyclonic circulation seen in southeastern BoB in the surface current is associated with the presence of anti-cyclonic eddy over this region, which extends vertically to thermocline depth. This signature can be seen most prominently in the anti-cyclonic circulation in the thermocline current over this region in the regional simulations (Figure 15c,e,g). Among the reanalysis products, this anti-cyclonic circulation can be seen in SODA3 and GODAS, but is almost absent in ORAS5. It is to be noted that below 200 m,this anticyclonic eddy is absent in all simulations (not shown). This implies that the vertical extent of anti-cyclonic eddy over southwest BoB is upto the upper thermocline. The thermocline current structure in the western BoB is different than its surface structure. Marked differences can be seen in eastern and southern BoB (Figure 12 and 15). The weak anti-cyclonic circulation in the southern BoB in the surface current becomes very prominent at the thermocline depth (Figure 12 and 15). Another feature is the presence of an eastern boundary current along the coast at thermocline depth, which is completely absent at the surface. This thermocline current could have been triggered by the propagating coastal Kelvin waves generated at the eastern Equatorial Indian Ocean by eastward propagating equatorial Kelvin waves (Rao et al., 2010). Although in this study we did not analyzed the SLA from these experiments, the SLA from Exp-1 shows clear Kelvin wave propagation(see Figures 11 and 14 in Rahaman et al., 2014). This coastally trapped thermocline current is not very prominent in the reanalysis products except GODAS which shows its presence with broader width (Figure 15d,f,h).

In July, the circulation at thermocline depth in the BoB more or less resembles the mixed layer current pattern. The boundary currents in northern BoB and east of Andaman Island are very prominent in the regional models (Figs. 16c,e,g) but almost absent in the reanalysis products (Figs.16d,f,h). The northeastward SMC current east of Sri Lanka seen atthe surface is very strong (~ 70 cm/s) and is also present at the thermocline depth, but with reduced

speed (~ 25 cm/s). This strong current mostly transports the high salinity water into the BoB from Arabian Sea via the equatorial Indian Ocean. In November, even at the thermocline depth, the EICC structure is very prominently seen. But currents in the interior Bay are different than mixed layer currents (not shown).

3.3 Salt Transport at 8 °N

The analysis in the previous section shows that the regional simulation in Exp-3 is able to capture the upper ocean mean and variability of temperature, salinity, and currents with good accuracy. Now, in this section, we discuss the seasonal and inter-annual salt transport into and out of BoB. It has been reported in earlier studies that during the summer monsoon the highly saline AS water intrudes into the south BoB (Schott et al., 1994;Vinaychandran et al., 1999,2013). Recent studies shows that the high salinity water enters the BoB centered between 75 -130 m depth along 83-90 °E (Sanchez-Franks et al., 2019). Most of the studes on salt transport into BoB are concentrated in the upper oceans (0-400 m), Vinayachandran et al. (1999,2013,2018). However, below 400 m,at what depth it occurs and how much is the salt flux is not known from previous studies. We have therefore computed the salt transport along 8 ^{o}N upto 2000 m depth,as described in Section 2.

Before computing salt trasport we show the mean and monthly standard deviation meridional current from all three regional simulations and three reanalysis products along the 8 °N (Figs. 17, 18). Mean meridional current is week below 100 m in all simulations (Fig. 17). All simulations show equatorward (poleward) currents along 80-84 °E (84-88°E) in the upper 100 m. This structure resembles the EICC and SMC currents, and in ORAS5 the meridional current speed is stronger as compared to other products. The presence of strong northward current along 82-84 °E up to~1500 m can be seen in ORAS5. This deeper current is also present in all regional models, but its magnitude is weak (Fig. 17). The standard deviation of the meridional current is shown in Figure 18. The variability is large along the EICC path up to 1500 m depth,with large values near the mixed layer. Regional model simulations matches ORAS5 STD distribution. The varibility near the surface is also large in all simulations, but in GODAS its magnitude is too high. It is to be noted that the STD values along the EICC pathways is larger than its mean for the meridional current (Figs. 17,18).

From the above analysis, we can see that regional model simulations with improved initial and open lateral boundary conditions, i.e., Exp-3, reproduces the temperature, salinity and circualtion in the BoB with good accuracy. Hence, we used Exp-3 for estimating the salt trasport into (out) the BoB from Arabian Sea. Figure 19 shows the seasonal average salt transport in the upper ocean (0-2000 m) across 8 °N. During winter, southward salt transport (~ 4 psu-m/s) is observed along 82 °E up to 1000 m depth, with a maximum in the narrow surface layer (Figure 19a). This southward transport is associated with the EICC which is most prominent during Nov-Dec. The surface layers of the rest of the basin (82-92 °E) show northward transport, most prominent in the east of EICC. This result corroborates the observation-based findings of Wijesekera et al.(2015). It shows that the EICC is approximately 100 km wide, with speeds exceeding 1 m/s in the upper 75 m and east of the EICC, a subsurface-intensified, 300 km-wide, northward current is observed, with maximum speeds as high as 1 m/s between 50 m and 75 m. It is interesting to note that west of 82 °E, there exists a very thin surface layer that shows southward transport in the mixed layer. In the upper 100 m below this layer, a band of northward transport in the thermocline region can be seen. Further below this layer from 100 m depth, a much deeper southward transport can be seen. The existence of these three narrow currents has been reported in hydrographic observations by Shetye et al. (1996) (their Figure 13).Wijesekera et al. (2015) with more recent observations andGordon et al.(2016) using model simulations show that Arabian Sea water also enters the BoB as a subsurface flow during the northeast monsoon season (December to March). Both these observational and modelling studies show a persistent northward flow of high-salinity water (>34.5 psu) found between 82 °E and 85 °E from December to February (DJF) at 50 m depth. This study shows similar features but it also shows a subsurface salt flux along 96 °E to 98 °E at 0-50 m depth, which has not been reported in both these earlier studies (Fig. 19a). This northward trasnport could be due to the presence of northward current over this region (Fig. 14g). Presence of similar northward current in May 2016 has been reportted by Webber et al., 2018 (see their figure 12a)

In spring, large salt flux towards the equator in a narrow band off Sri Lanka is observed with a peak in the thermocline is observed (~ 8 psu-m/s). This southward salt flux is associated with the strong narrow southward current observed in the thermocline (Fig. 15g). East of this southward salt flux, a strong northward salt flux is seen in the thermocline as

well. Very weak southward transportis seen on the surface (west of 90 °E) and also in the deeper ocean below 400 m (west of 90 °E) (Figure 19b).

During summer, it can be seen that the core of the salt transport (salt flux ~12 psu-m/s) lies below the mixed layer at around 50-150 m depth along 84 °E. Earlier studies also reported salt transport at similar depth and location (Vinayachandran et al. 1999,2013;. Sanchez-Franks et al. 2019; Sheehan et al.,2020; Jensen et al., 2016). Webber et al. (2018) reported northward transport ranging between 16.7 and 24.5 Sv during July 2016 using data from high-resolution in situ measurements along an east–west section at 8 °N in southern BoB. However, all these studies focused on the upper 250 m. We have found another deeper path for salt intrusion at 300-1500 m depth along 82 °E (Figure 19c). This deeper trasport is associated with the deeper currents presents along the coast. Hydrographic survey showed the presence of a boundary current EICC between 81°E and 82 °E up to 300 m depth(Shcherbinin et al., 1979). Further a series of hydrographic surveys (Shetye et al. 1991b, 1993, 1996) showed that during February–May, EICC extends to greater depths than during the summer-monsoon months of June–August, when the poleward EICC is shallow (∼70 m deep) (Shetye et al. 1991b,1993,1996). However, the presence of EICC transport to 1000 m depth was reported by Shetye et al. (1991b). All these observations are north of 10 °N. South of this, the bathymetry shows a steep slope and a very narow shelf. The well defined strong current along the east coast of Sri Lanka follows the bathymetry (Rahaman et al. 2014)

It is also observed that during summer, along the coast,salt is transported southward in the mixed layer. The magnitude of the salt flux is ~ 12 psu-m/s,the same order as subsurface northward transport. Southward transport is also observed along 88-95 °E in the entire upper ocean with a core at 96 °E in the upper 100 m.

Significant northward salt transport was also observed during fall in the upper ocean (50-400 m), just below the mixed layer along the coast of Sri Lanka along 82-83 °E (Fig. 19d). The southward salt flux of ~ 2-6 psu-m/s is observed during fall in a narrow band of 10-20 m depth and also below 400 m depth along the east coast of Sri Lanka. This southward salt transport along the east coast of Sri Lanka is seen in all seasons with varying magnitudes, with a maximum in summer and a minimum in spring in the mixed layer just east of Sri Lanka. Significantly large salt flux (16 psu-m/s)north of 14 °N can be seen along the east

coast of India during spring and is associated with the EICC(not shown). The reversal of this salt transport during fall also has a similar magnitude (salt flux of 16 psu-m/s) (not shown).

Figure 20 shows the time series of inter-annual variation of depth-integrated salt transport across 8 °N during 2003-2009. The upper ocean (0-200 m) salt transport shows peak northward transport during Apri-May and November-December of each year with large inter-annual variability (Figure 20a). It is southward during June-July again with large inter-annulal variations,but with much reduced magnitude during IOD year 2006. The southward salt transport during summer monsoon is due to the Ekman transport associated with SMC (Schott and McCreary, 2001;Vinayachandran et al.. 1999). This southward salt transport is mainly confined to the Sri Lanka coast and east of 90 °E (Fig.19c). In the upper ocean (0-200 m), salt transport shows very prominent inter-annual variation broadly consists of two peaks, one in spring and another in autumn (Figure 20a). In the top 1000 m, there is also a marked inter-annual variability similar to the top 200 m transport (Figure 20b). Presence of prominent intra-seasonal variability can be seen when integrating transports over the top 2000 m (or over the full depth) (Figure 20c,d). This intra-seasonal variability is more active in some years than others (i.e. it varies inter-annually). The transport for the entire depth also shows large inter-annual variability. It is worth mentioning that the full-depth transports are much weaker than the variability shown for 0-200, 0-1000 and 0-2000 m. The largest variability is seen for 0-1000 m and the values decrease when the vertical integral covers the top 2000 m (or the full depth). This suggests a degree of compensation between the variability above and below 1000 m. Unlike prominant seasonal cycle in upper ocean upto 1000 m depth, transport upto deeper depth shows more prominent intra-seasonal componenet as well (Fig. 20c,d). The reason could be due Eastward-propagating oceanic equatorial Kelvin waves forced by Madden-Julian Oscillation, observed, using the Argo array of profiling floats (Matthews et al. 2007), to extend downward to 1500 m and having larger amplitude than the annual cycle. They have shown that the amplitude of the deep ocean anomalies is up to six times the amplitude of the observed annual cycle. It is worth mentioning that when this equatorial Kelvin wave reaches the Sumatran Coast, it triggers north ward propagating coastal Kelvin wave into the Bay of Bengal (Rao et al., 2010). Heywood et al. (1994) have reporthed a 50-day oscillation in the observed currents down to 3000 m depth in the Indian Ocean,

738 consistent with a zonally propagating Rossby wave. However, more detailed analysis is
739 required to find out the exact reason for the prominent intraseasonal variation of deeper salt
740 trasport, which is beyond the scope of this study.
741
742 The upper ocean (0-200 m) seasonal mean salt transport (Table -1) is northward in all
743 seasons (MAM :72 psu-m^3/s, SON:42 psu-m^3/s, DJF :12 psu-m^3/s), except during the
744 summer monsoon when it is southward (-99 psu-m^3/s). The total depth-integrated transport is
745 also southward during the monsoon season (JJA: -23 psu-m^3/s) and during fall (SON: -17
746 psu-m^3/s). It can be seen that large variability exists in the seasonal transport (Table 1). In all
747 other seasons, the STD values are much higher in the upper ocean (0-200 m), compared to
748 its mean. Other depth-averaged values are similar, except in SON. For example, during
749 winter (DJF), the transport is southward for January-February of 2004,2005 and 2006, with
750 the highest(lowest) value of -155 psu-m^3/s (-29 psu-m^3/s) in January 2004(2005)but
751 northward in 2003 and 2007. The transport during Spring (MAM) is mostly northward, with
752 peak values reached in either April or May and with the highest transport (300 psu-m^3/s) in
753 May 2004. However,in some years, the transport is southward, also with a peak value of 120
754 psu-m^3/s in March 2006. The mean Fall transport is also northward, with a southward
755 transport in either September or October with a large inter-annual variation. November
756 transport is northward in all years with a range of 30-309 psu-m^3/s. The mean depth-averaged
757 transport is however southward during Fall.
758 In order to see transport variability with depth we show Hovmollar (depth vs time) plot in
759 the upper ocean (0-500 m) in Figure 21. A strong seasonal salt transport confined up to 50 m
760 depth can be seen. As shown in the time series plots during winter (summer) the strong
761 northward (southward) transport is confined upto 50 m depth. The contribution in the strong
762 nortward transport during April-May as shown in Figure 20a is mostly from 50 -150 m
763 depths.
764
765 **4. Summary and Conclusions**
766 Accurate initial and lateral boundary conditions are essential for realistic simulations of
767 the water mass structure and currents in any regional ocean model. One way nesting of the
768 regional model with a global model is one of the techniques to overcome the lateral boundary

condition issue. We have demonstrated this by performing three experiments using a nested Indian Ocean regional model (see details about the model configuration in Rahaman et al., 2014). We performed three experiments in Exp-1 we used initial and lateral boundary conditions from the original nested global model. In Exp-2 we used initial conditions from INCOIS-GODAS reanalysis, but lateral boundary conditions were the same as Exp-1 and, finally in Exp-3 we used both initial and lateral boundary conditions from INCOIS-GODAS reanalysis.

Of the three experiments (Exp-1,Exp-2 and Exp-3) we conducted, the one with accurate initial and lateral boundary conditions (Exp-3) provided the best agreement of temperature and salinity fields with co-located and concurrent Argo profiling floats observations. The mean and variability in terms of standard deviation of the upper ocean temperature and salinity are drastically improved in Exp-3.The mean bias of 3-4 °C in Exp-1 in the thermocline is reduced to 1.5 -2 °C in Exp-2 and furthermore to 0.5 -1.5 °C in Exp-3. Similarly, the upper ocean (0-500 m) mean bias in Exp-1 is 2.1 °C, which reduced to 1.1 °C in Exp-2 and only 0.41 °C in Exp-3. The mean salinity bias in Exp-1 is 0.01 psu, which is slight saltier compared to Argo observationsbecome slight fresh with mean bias of -0.11 psu and -0.09 psu in Exp-2 and Exp-3 respectively. Comparison with gridded salinity and temperature observations also shows similar improvement in the BoB.

Needless to say, that in addition to accurate water mass structure, another prerequisite for accurate simulations of narrow, energetic coastal currents is high horizontal spatial resolution in the model, coupled with correspondingly accurate bathymetry. We compared surface currents from all three simulations (Exp-1,Exp-2, and Exp-3) and three reanalysis products (GODAS,SODA3 and ORAS5). We used OSCAR analysis, which is widely used for the surface current variability and model evaluation studies, as a reference and also another analysis product SCUD. The mean spatial pattern of surface currents in the regional model simulations are more realistic than reanalysis products (GODAS,SODA3 and ORAS5), when compared with OSCAR and SCUD observations. In all reanalysis products, boundary currents (EICC and WICC) are weak and wide compared to OSCAR and SCUD observations, whereas in the regional model simulations, they are more realistically reproduced.Of all the three simulations, Exp-3 provides the best simulation of coastal currents in BoB, as suggested by good agreement of meridional currents in central and

southern BoB with the geostrophic currents computed with temperature and salinity computed from CORA5.2 observations and Exp-3 simulations. The spatial pattern of monthly variability (standard deviation) is also captured by all regional simulations but is most realistic in Exp-3,compared to reanalysis products (GODAS, SODA3 and ORAS5). Summer Monsoon Current (SMC), which is the key circulation feature through which the salty Arabian Sea water mass enters BoB and maintains salt balance in the BoB (Jensen, 2011; Vinayachandran et al., 2013) is most realistic in Exp-2 and Exp-3,when compared with OSCAR and SCUD. Reanalysis products capture the observed spatial structure but they underestimate SMC speed.

We found the effect of improvement in temperature and salinity at the thermocline depth in the thermocline current as well. The presence of anti-cyclonic gyre associated with the warm core anti-cyclonic eddy in western BoB off the east coast of India is most prominent in Exp-2 and Exp -3. The geostrophic current also shows the presence of this anti-cyclonic eddy.This anti-cyclonic eddy is absent in ORAS5 probably due to its coarse resolution (1 degree). Its presence is seen in SODA3 and GODAS but with weak circulation. We also discovered a narrow band of coastal currents flowing along the east coast of BoB during spring and summer at the thermocline depth. In April, thermocline currents reveal a narrow band of poleward currents along the north and east coast of BoB possibly driven by coastal Kelvin wave. This boundary current is most defined in Exp-2 and Exp-3 and weaker in Exp-1. GODAS and ORAS5 reanalysis products also show the presence of this but is completely absent in SODA3. This boundary current changes its direction towards the equator in July and again only prominently seen in regional simulations and absent in reanalysis products. In all regional simulations, it appears as a loop current present in almost the entire BoB along its boundary except for a small stretch of southwest BoB. It is worth mentioning that the coastally trapped Kelvin wave is well reproduced in Exp-1 (see more details in Rahaman et al. 2014). Along 94 °E and 12-16 °N, a narrow current enters Andaman Sea from northern BoB. Kiran (2017) has shown the presence of a strong flow through a shallow (250 m) channel named Preparis Channel (PC), which separates South Myanmar from North Andaman. The strong current in the regional simulations is due to realistic bathymetry and is absent in all reanalysis products. The regional simulations also show strong flow out of Andaman Sea along 93 °E centered at 10 °N towards equator. This flow is also present only

in the regional simulations. This also may be due to the realistic representation of ten degree channel in the regional model which is 600 m deep and lies between Little Andaman and Car Nicobar (Kiran 2017). As expected, the reanalysis products do not show this flow. In many earlier studies, it has been shown that 8 °N is the gateway to BoB basin. The SMC is an eastward jet along 8 °N between 85 and 92 °E present during the SW monsoon and peak velocity can exceed 1.5 m s^{-1}. Associated with this SMC northward transport has been estimated to be in the range 10–27 Sv (1Sv ≡ 10^6 m^3 s^{-1}), (Wijesekera et al. 2016; Vinayachandran et al. 1999; Webber et al. 2018). This estimation has uncertainty and is an overestimate due to the presence of recirculation (Cherian et al. 2020).

Accurate simulation of currents in the water column, especially the narrow, energetic coastal currents, results in better estimation of salt transport into and out of BoB. We found that apart from summer and inter-monsoon, significant salt transport also occurs in Spring and Fall particularly near the coast of Sri Lanka. This study also found that during the peak of summer, significant salt transport into the BoB occurs across 8 ^oN in the 300-1500 m layer depth. The salt transport during the monsoon season shows a core along 84 °E with peak values of ~8 psu-m^3/s just below the mixed layer (50-200 m). The upper ocean depth-averaged (0-200 m) salt transport shows prominent seasonal cycle with large inter-annual variability, with peak northward transports occurs during spring (Apr-May) and early winter (Nov-Dec). However, during the summer monsoon it is southward. Most prominent transport is confined to 50 m depth. In the deeper layers, apart from seasonal cycle, intra-seasonal cycle also is prominent upto 2000 m and at all depths.

We hope that these new findings, such as the narrow band of coastal currents along the east coast of India at the thermocline depth and salt transport below 250 m depth may provide new insights into the understanding of BoB circulation and its role in better predictions of the Indian summer Monsoon.

5. Acknowledgement

The authors thank the Director, Indian National Centre for Ocean Information Services (INCOIS) and the data set producer for the free access of these data sets. This is INCOIS contribution no. xxxx. LK acknowledges support by ONR Grant # N00014-17-1-2716. We thank the anonymous reviewer and the editor for their valuable comments with which the

862 mnauscript improved considerably. All the figures were made using FERRET and
863 ORIGIN6.1 software. The reanalysis data sets SODA3.3.1 and ORAS5 and the observational
864 data sets SLA OSCAR and SCUD are obtained from http://apdrc.soest.hawaii.edu/index.php
865
866 **References**
867

868 Alves, O., Balmaseda, M. A., Anderson, D., Stockdale, T., 2004.Sensitivity of dynamical
869 seasonal predictions to ocean initial conditions. Quart. J.Roy.Meteorol. Soc., 130, 647–
870 667.
871 Anutaliya, A., Send, U., McClean, J. L., Sprintall, J., Rainville, L., Lee, C. M., Jinadasa, S.
872 U. P., Wallcraft, A. J.,Metzger, E. J.,2017. An undercurrent off the east coast of Sri
873 Lanka, Ocean Sci., 13, 1035–1044, https://doi.org/10.5194/os-13-1035-2017.
874 Balmaseda, M. A., Anderson, D., 2009. Impact of initialization strategies and observations
875 on seasonal prediction skill. Geophys. Res. Lett., 36, L01701.
876 https://doi.org/10.1029/2008GL035561
877 Balmaseda M.A., Mogensen, K., Weaver, A.T., 2013. Evaluation of the ECMWF ocean
878 reanalysis system ORAS4. Quart. J.Roy.Meteorol. Soc., 131:1132–1161.
879 Balmaseda, M.A., Hernandez, F., Storto, A., Palmer, M.D., Alves, O., Shi, L., Smith, G.C.,
880 Toyoda, T., Valdivieso, M., Barnier, B., Behringer, D., Boyer, T., Chang, Y.S.,
881 Chepurin, G.A., Ferry, N., Forget, G., Fujii, Y., Good, S., Guinehut, S., Haines, K.,
882 Ishikawa, Y., Keeley, S., Köhl, A., Lee, T., Martin, M., Masina, S., Masuda, S.,
883 Meyssignac, B., Mogensen, K., Parent, L., Peterson, K.A., Tang, Y.M., Yin, Y. ,
884 Vernieres, G., Wang, X., Waters, J., Wedd, R., Wang, O., Xue, Y., Chevallier, M.,
885 Lemieux, J.F., Dupont, .F.,Kuragano, T., Kamachi, M., Awaji, T., Caltabiano, A.,
886 Wilmer-Becker, K., Gaillard, F., 2015. The Ocean ReanalysesIntercomparison Project
887 (ORA-IP). J Oper.Oceanogr. 8, 80–97.
888 http://dx.doi.org/10.1080/1755876X.2015.1022329
889
890 Barth, A., Alvera-Azcárate, A., Rixen, M., Beckers, J.M., 2005. Two-way nested model of
891 mesoscale circulation features in the Ligurian Sea. Prog. Oceanogr. 66, 171– 189.

892 Behringer, D. W., 2007: The Global Ocean Data As-similation System (GODAS) at NCEP.
893 Preprints, 11th Symp. on Integrated Observing and Assimila-tion Systems for
894 Atmosphere, Oceans, and Land Surface, San Antonio, TX, Amer. Meteor. Soc., 3.3.
895 [Available online at http://ams.confex.com/ams/pdfpapers/119541.pdf.]
896 Bonjean, F., Lagerloef, G.S.E., 2002. Diagnostic Model and Analysis of the Surface Currents
897 in the Tropical Pacific Ocean. J. Phys. Oceanogr. 32, 2938–2954.
898 https://doi.org/10.1175/1520-0485(2002)032<2938:DMAAOT>2.0.CO;2
899
900 Bharti, D. K., Guizien,K., Aswathi-Das,M. T., Vinayachandran, P. N., Shanker, K.,2021.
901 Connectivity networks and delineation of distinct coastal provinces along the Indian
902 coastline using large-scale Lagrangian transport
903 simulations.bioRxiv 2021.04.24.441108; https://doi.org/10.1101/2021.04.24.441108
904 Bradley, E.F., Weller R.A., 1995.Third Workshop of the TOGA COARE Air- Sea Interaction
905 (Flux) Working Group, 2-4 August, 1995, University of Hawaii,Honolulu, HI. TOGA
906 COARE International Project Office, UCAR, Boulder, CO, 34 pp.
907 Carton, J. A., Giese., B. S., 2008. A reanalysis of ocean climate using Simple Ocean Data
908 Assimilation (SODA). *Mon. Wea. Rev.*, **136**, 2999–3017.
909 https://doi.org/10.1175/2007MWR1978.1.
910 Carton, J. A., Chepurin, G., Cao,X., Giese,B. S., 2000a. A Simple Ocean Data Assimilation
911 analysis of the global upper ocean 1950–95. Part I: Methodology. *J. Phys.*
912 *Oceanogr.*, **30**, 294-309.
913 https://doi.org/10.1175/15200485(2000)030<0294:ASODAA>2.0.CO;2.
914 Carton, J. A., Chepurin,G., Cao, X., 2000b.A Simple Ocean Data Assimilation analysis of
915 the global upper ocean 1950–95. Part II: Results. *J. Phys. Oceanogr.*, **30**, 311–326.
916 https://doi.org/10.1175/1520-0485(2000)030<0311:ASODAA>2.0.CO;2.
917 Carton, J. A., Chepurin, G. A., Chen, L., 2018. SODA3: A New Ocean Climate
918 Reanalysis, J. Clim, 31(17), 6967-6983.
919 https://journals.ametsoc.org/view/journals/clim/31/17/jcli-d-18-0149.1.xml
920
921 Cabanes, C., Grouazel,A., von Schuckmann, K., Hamon,M., Turpin,V., Coatanoan, C.,
922 Paris,F., Guinehut, S., Boone, C., Ferry, N., de Boyer Montégut, C., Carval,T.,
923 Reverdin, G., Pouliquen,S., Le Traon, P. Y., 2013. The CORA dataset: validation and

924 diagnostics of in-situ ocean temperature and salinity measurements. Ocean Sci, 9, 1-
925 18, http://www.ocean-sci.net/9/1/2013/os-9-1-2013.html, doi:10.5194/os-9-1-2013.
926 Capotondi, A., Alexander, M. A., Bond,N. A., Curchitser,E. N., Scott, J. D., 2012, Enhanced
927 upper ocean stratification with climate change in the CMIP3 models, J. Geophys.
928 Res.,117, C04031, doi:10.1029/2011JC007409
929 Cailleau, S., Fedorenko, V., Barnier, B., Blayo, E., Debreu, L., 2008. Comparison of different
930 numerical methods used to handle the open boundary of a regional ocean
931 circulationmodel of the Bay of Biscay. Ocean Modell. 25, 1–16.
932 Cherian, D. A., Shroyer, E. L., Wijesekera, H. W., Moum, J. N., 2020. The Seasonal Cycle of
933 Upper-Ocean Mixing at 8°N in the Bay of Bengal, J. Phys. Oceanogr, 50(2), 323-342.
934 https://journals.ametsoc.org/view/journals/phoc/50/2/jpo-d-19-0114.1.xml
935 Cooper, N. S., 1988.The effect of salinity on tropical ocean models, J. Phys.
936 Oceanogr., 18, 697–707.
937 Cutler A.N., Swallow J.C. Surface currents of the Indian Ocean, (to 25øS, 100øE), Vol.
938 187: Tech. Rep. Inst. of Oceanogr. Sci., Wormley, Godaiming, Surrey, England (1984),
939 p. 8 36 charts
940 Dai, A., Trenberth,K. E., 2002. Estimates of freshwater discharge from continents:Latitudinal
941 and seasonal variations. J. Hydrometeorol., 3, 660-687.
942 Daryabor, F., Ooi, S.H., Samah, A.A., Akbari, A., 2016. Dynamics of the Water Circulations
943 in theSouthern South China Sea and Its Seasonal Transports. PLoS ONE 11(7):
944 e0158415. doi:10.1371/journal.pone.0158415.
945 Debreu, L., Blayo, E., 2008. Two-way embedding algorithms: a review. Ocean Dyn. 58, 415–
946 428.
947 deBoyerMontégutet, C., Vialard, J., Shenoi, S.S.C., Shankar, D., Durand, F., Ethé, C.,
948 Madec, G., 2007. Simulated seasonal and interannual variability of mixed layer heat
949 budget in the northern Indian Ocean. J. Clim. 20, 3249-3268.
950 Durand, F., Shankar,D., de Boyer Montégut, C., Shenoi,S. S. C., Blanke,B., Madec, G., 2007.
951 Modeling the barrier-layer formation in the South-E*wastern Arabian Sea, J.Clim, 20,
952 2109-2120.
953 Eigenheer, A., Quadfasel D., 2000, Seasonal variability of the Bay of Bengal circulation
954 inferred from TOPEX/Poseidon altimetry, J. Geophy.Res, 105, 3243–3252.

955 Gopalakrishna, V. V., Murty, V. S. N., Sengupta,D., Shenoy,S., Araligidad, N., 2002. Upper
956 ocean stratification and circulation in the northern Bay of Bengal during the southwest
957 monsoon of 1991, Cont. Shelf Res., 22, 791– 802.
958 Gopalakrishna, V. V., Johnson,Z., Salgaonkar, G., Nisha, K., Rajan,C. K., Rao, R. R.,
959 2005.Observed variability of sea surface salinity and thermal inversions in the
960 Lakshadweep Sea during contrast monsoons, Geophys. Res. Lett., 32, L18605,
961 doi:10.1029/2005GL023280.
962 Gordon, A. L., 2001.Interocean exchange in Ocean Circulation and Climate, edited by G.
963 Siedler, J. Church, and J. Gould, 303– 314, Elsevier, New York.
964 Gordon, A.L., Shroyer,E.L., Mahadevan,A., Sengupta, D., Freilich, M., 2016. Bay of Bengal:
965 2013 northeast monsoon upper-ocean circulation. Oceanography 29(2):82–91.
966 http://dx.doi.org/10.5670/oceanog.2016.41.
967 Griffies, S.M., 2009. Elements of MOM4P1 GFDL Ocean Group Technical Report No. 6
968 NOAA/Geophysical Fluid Dynamics Laboratory, 444 p.
969 Gopalakrishnan, G., and B.D. Cornuelle. 2019. Palau's effects on regional-scale ocean
970 circulation. Oceanography 32(4):126–135, https://doi.org/10.5670/ oceanog.2019.418.
971 Han, W., McCreary, J. P., 2001. Modeling salinity distributions in the Indian Ocean, J.
972 Geophys. Res., 106, 859–877
973 Han, W., McCreary, J.P., Kohler, K.E., 2001. Influence of precipitation minus evaporation
974 and Bay of Bengal rivers on dynamics, thermodynamics, and mixed layer physics in the
975 upper Indian Ocean. J. Geophys. Res. Oceans 106, 6895–6916.
976 https://doi.org/10.1029/2000JC000403
977 Halliwell, G. R., Jr., Shay, L. K., Brewster, J. K., Teague, W. J., 2011. Evaluation and
978 Sensitivity Analysis of an Ocean Model Response to Hurricane Ivan, Mon. Weather
979 Rev., 139(3), 921-945 10.1175/2010MWR3104.1
980
981 Herzfeld, M., Schmidt, M., Griffies, S.M., Liang, Z., 2011. Realistic test cases for limited
982 area ocean modelling. Ocean Model. 37, 1–34.
983 Heywood K. J., E. D. Barton, G. L. Allen, 1994. South Equatorial Current of the Indian
984 Ocean: Fifty-day oscillation Oceanol. Acta 17, 255
985

Huang, B., Xue, Y.,Behringer, D. W., 2008. Impacts of Argo salinity in NCEP global ocean data assimilation system: The tropical Indian Ocean. J. Geophys. Res., 113, C08002. https://doi.org/10.1029/2007JC004388

Jain,V., . Shankar, D.,Vinayachandran,P.N., Kankonkar, A., Chatterjee,A., Amol,P., Almeida,A.M., Michael, G.S., Mukherjee, A., Chatterjee,M., Fernandes,R., Luis,R., Kamble, A., Hegde, A.K, Chatterjee, S. , Das,U., Neema, C.P., 2017. Evidence for the existence of Persian Gulf water and Red Sea water in the Bay of Bengal.Clim. Dyn., 48 , 3207-3226, 10.1007/s00382-016-3259-4

Jensen, T. G., 1991.Modeling the seasonal undercurrents in the Somali Current System, J. Geophys. Res., 96, 22,151–22,167,

Jensen, T. G., 2001.Arabian Sea and Bay of Bengal exchange of salt and tracers in an ocean model, Geophys. Res. Lett.,28(20), 3967–3970, doi:10.1029/2001GL013422.

Jensen, T. G., 2003. Cross-equatorial pathways of salt and tracers from the northern Indian Ocean: Modelling results, Deep Sea Res., Part II, 50, 2111 – 2127.

Jensen, T.G., Wijesekera,H.W., Nyadjro,E.S., Thoppil,P.G., Shriver,J.F., Sandeep,K.K., Pant, V., 2016. Modeling salinity exchanges between the equatorial Indian Ocean and the Bay of Bengal. *Oceanography* 29(2):92101, https://doi.org/10.5670/oceanog.2016.42.

Kantha L, Rojsiraphisal,T., Lopez,J., 2008.The North Indian Ocean circulation and its variability as seen in a numerical hindcast of the years 1993–2004,Progr. Oceanogr.,76,(1), 111-147.

Jithin, A. K., Francis,P. A., Unnikrishnan, A. S., Ramakrishna, S. V. S. S., 2019. Modeling of internal tides in the western Bay of Bengal: characteristics and energetics. J.Geophy. Res.Oceans,124:1–27. https://doi.org/10.1029/2019JC015319

Jouanno, J., Sheinbaum, J., Barnier, B., Molines, J.M., Debreu, L., Lemarie, F., 2008. The mesoscale variability in the Caribbean Sea. Part I: Simulations and characteristics with an embedded model. Ocean Modell. 23, 82–101.

Kiran S.R., 2017. General Circulation and Principal Wave Modes in Andaman Sea from Observations Indian J.Sci. Tech., 10(24), DOI: 10.17485/ijst/2017/v10i24/115764, ISSN (Print) : 0974-6846 ISSN (Online) : 0974-5645https://arxiv.org/ftp/arxiv/papers/2103/2103.09771.pdf

Kurian, J., Vinayachandran, P.N., 2007. Mechanisms of formation of the Arabian Sea mini warm pool in a high-resolution Ocean General Circulation Model. J. Geophys. Res. 112. https://doi.org/10.1029/2006JC003631

Lee, T., Fukumori, I., Menemenlis, D,. et al. 2002. Effects of the Indonesian throughflow on the Pacific and Indian oceans.J.Phys.Oceanogr., 32:1404–1429. https://doi.org/10.1175/1520-0485(2002)032<1404:Eotito>2.0.Co;2

Lellouche, J.-M.,Greiner, E.,Le Galloudec, O.,Garric, G.,Regnier, C.,Drevillon, M., etal. 2018.Recent updates to the Copernicus Marine Service global ocean monitoring and forecasting real-time 1⁄12° high-resolution system. Ocean Science, 14, 1093–1126. https://doi.org/10.5194/os-14-1093-2018

Li, Yuanlong., Wang, F., 2014. Thermocline spiciness variations in the tropical Indian Ocean observed during 2003–2014, Deep Sea Research Part I: Oceanogr. Res. Papers, 97, 52-66, ISSN 0967-0637, https://doi.org/10.1016/j.dsr.2014.12.004.

Llovel, W., Lee, T., 2015. Importanceand origin of halosteric contribution tosea level change in the southeast Indian Ocean during 2005–2013,Geophys. Res.Lett.,42, 1148–1157, doi:10.1002/2014GL062611.

Marchesiello, P., McWilliams, J.C., Shchepetkin, A., 2001. Open boundary conditions for long term integration of regional oceanic models. Ocean Modell. 3, 1–20.

Matthews, A. J., Singhruck, P. & Heywood, K. J. 2007. Deep ocean impact of a Madden-Julian Oscillation observed by Argo floats.*Science* **318**, 1765–1769.

Meehl, G.A., Richter, J.H., Teng, H. *et al.* 2021. Initialized Earth System prediction from subseasonal to decadal timescales. *Nat Rev Earth Environ* **2,** 340–357. https://doi.org/10.1038/s43017-021-00155-x

Maximenko, N.A., Hafner,J., 2010. *SCUD: Surface Currents from Diagnostic model,* IPRC Tech. Note 5, 17pp.

McPhaden, M. J., Meyers, G., Ando, K., Masumoto, Y., Murty, V. S. N., Ravichandran, M., et al. (2009). RAMA: The research moored array for African-Asian-Australian monsoon analysis and prediction. Bull. Am. Meteorol. Soc. 90, 459–480. doi: 10.1175/2008BAMS2608.1

1046 Miyama, T., McCreary Jr., J. P., Jensen,T. G., Loschnigg,J., Godfrey,J. S., Ishida, A., 2003.
1047 Structure and dynamics of the Indian-Ocean cross equatorial cell, Deep Sea Res., 50,
1048 2023–2047.
1049 Mukherjee, A., Shankar, D., Chatterjee, A. et al. 2018.Numerical simulation of the observed
1050 nearsurface East India Coastal Current on the continental slope. Clim.Dyn., 50, 3949–
1051 3980.https://doi.org/10.1007/s00382-017-3856-x
1052 Murtugudde, R., Busalacchi, A.J., 1999. Interannual variability of the dynamics and
1053 thermodynamics, and mixed layer processes in the Indian Ocean.J. Clim, 12, 2300–
1054 2326.https://doi.org/10.1175/1520-0442(1999)012
1055 Nyadjro, E. S., Subrahmanyam, B., Murty, V. S. N., Shriver,J. F., 2010. Salt transport in the
1056 nearsurface layer in the monsooninfluenced Indian Ocean using HYCOM.Geophys. Res.
1057 Lett., 37, L15603, doi:10.1029/ 2010GL044127
1058 Nyadjro, E. S., Subrahmanyam,B. , Shriver,J. F., 2011. Seasonal variability of salt transport
1059 during the Indian Ocean monsoons. J. Geophys. Res., 116, C08036,
1060 doi:10.1029/2011JC006993.
1061 Nyadjro, E. S., Subrahmanyam,B., Giese B. S., 2013. Variability of salt flux in the Indian
1062 Ocean during 1960-2008. Remote Sensing of Environment, 134, 175-193.
1063 Penven, P., Debreu, L., Marchesiello, P., McWilliams, J.C., 2006. Evaluation and application
1064 of the ROMS 1-way embedding procedure to the central California upwelling system.
1065 Ocean Modell. 12, 157–187.
1066 Prasanna Kumar, S., Narvekar,J., Kumar,A., Shaji, C., Anand,P., Sabu, P., Rijomon,G.,
1067 Josia,J., Jayaraj,K. A., Radhika, A., Nair, K. K. C., 2004. Intrusion of the Bay of Bengal
1068 water into the Arabian Sea during winter monsoon and associated chemical and
1069 biological response, Geophys. Res. Lett.,31, L15304, doi:10.1029/2004GL020247.
1070 Rahaman, H., Ravichandran, M., Sengupta, D., Harrison, M.J., Griffies, S.M.,
1071 2014.Development of a regional model for the north Indian Ocean. Ocean Model. 75 1–
1072 19.
1073 Rahaman, H., Srinivasu,U., Panickal,S., Durgadoo,J.V., Griffies,S.M., Ravichandran, M.,
1074 Bozec,A., Cherchi , A., Voldoire,A., Sidorenko ,D ., Chassignet,E.P., Danabasoglu, G.,
1075 Tsujino, H., Getzlaff,K., Ilicak, M., Bentsen ,M., Long ,M.C., Fogli,P.G., Farneti, R.,
1076 Danilov , S., Marsland, S.J., Valcke,S., Yeager, S.G., Wang, Q., 2020, An assessment of

the Indian Ocean mean state and seasonal cycle in a suite of interannual CORE-II simulationsOcean Modell., 145, , 101503.
https://www.sciencedirect.com/science/article/pii/S1463500319301118?via%3Dihub
Rahaman, H., Venugopal, T., Penny,S.G., Behringer, D., Ravichandran,M., Raju,J .V .S., Srinivasu, U., Sengupta, D., 2018. Improved Ocean analysis for the Indian Ocean. J. Oper.Oceanogr. , DOI: 10.1080/1755876X.2018.1547261
Rahaman,H., Behringer,D., Penny,S.G., Ravichandran, M., 2016. Impact of an upgraded model in the NCEP Global Ocean Data Assimilation System: The tropical Indian Ocean. J. Geophys. Res. Oceans, 121, doi:10.1002/2016JC012056
Rao, R.R., Sivakumar, R., 2003. Seasonal variability of sea surface salinity and salt budget of the mixed layer of the north Indian Ocean. J. Geophys. Res. 108 (C1), 3009. http://dx.doi.org/10.1029/2001JC000907
Rao, R. R., Girishkumar,M. S., Ravichandran,M., Gopalakrishna, V. V., Thandahil, P., 2011. Do cold, low saline waters pass through the Indo-Sri Lanka Channel during winter? International J. Remote Sensing, doi: 10.1080/01431161.2010.523728. Vol. 32, No. 22, 7383–7398.
Rao,R.R., Girish Kumar, M.S., Ravichandran, M., Rao, A.R., Gopalakrishna, V. V., Thadathil, P .,2010. Interannual variability of Kelvin wave propagation in the wave guides of the equatorial Indian Ocean, the coastal Bay of Bengal and the southeastern Arabian Sea during 1993-2006. Deep-Sea Res., Part I: Oceanographic Research Papers, 57 (1), pp. 1-13.
Ravichandran, M., Behringer, D., Sivareddy, S., Girishkumar, M. S., Chacko, N., Harikumar, H., 2013. Evaluation of the global ocean data assimilation system at INCOIS: The tropical Indian Ocean, Ocean Modell., 69, 123–135, doi:10.1016/j.oceamod.2013.05.003
Sanchez Franks, Alejandra, et al. 2019 The railroad switch effect of seasonally reversing currents on the Bay of Bengal high salinity core. *Geophy.Res.Lett.,* 46.11 (2019): 6005-6014.
Sheehan, Peter MF, et al. 2020. Injection of oxygenated Persian Gulf Water into the southern Bay of Bengal." *Geophys. Res. Lett.,* 47.14 : e2020GL087773.

Shetye, S.R., Gouveia, A.D., Shenoi, S.S.C., Michael, G.S., Sundar, D., Almeida, A.M.,Santanam, K., 1991a. The coastal current of western India during the northeastmonsoon. Deep-Sea Res. I 38 (12), 1517–1529.

Shetye, S.R., Shenoi, S.S.C., Gouveia, A.D., Michael, G.S., Sundar, D., Nampoothiri, G.,1991b. Wind-driven coastal upwelling along the western boundary of the Bayof Bengal during the southwest monsoon. Cont. Shelf Res. 11 (11), 1397–1408.

Shetye, S.R., Gouveia, A.D., Shenoi, S.S.C., Sundar, D., Michael, G.S., Nampoothiri, G.,1993. The western boundary current of the seasonal subtropical gyre in Bay ofBengal. J. Geophys. Res. 98 (C1), 945–954.

Shetye S.R., Shenoi S.S.C. Seasonal cycle of surface circulation in the North Indian Ocean Proceedings of the Indian Academy of Sciences (Earth and Planetary Sciences), 97 (1988), pp. 53-62

Shetye, S.R., Gouveia, A.D., Shankar, D., Shenoi, S.S.C., Vinayachandran, P.N., Sundar, D., Michael, G.S., Nampoothiri, G., 1996. Hydrography and circulation in the western Bay of Bengal during the northeast monsoon. J. Geophys. Res. 101 (C6), 14,011–14,025.

Sengupta, D., Raj, G.N.B., Shenoi, S.S.C., 2006. Surface freshwater from the Bay of Bengal runoff and Indonesian throughflow in the tropical Indian Ocean. Geophys. Res. Lett. 33 (L22609), 2006G. http://dx.doi.org/10.1029/L027573

Schott, F., Reppin, J., Fischer, J., Quadfasel, D. 1994. Currents and transports of the Monsoon Current south of Sri Lanka, J. Geophys. Res., 99(C12), 25127– 25141, doi:10.1029/94JC02216.

Schott, F.A., McCreary, J.P., 2001. The monsoon circulation of the Indian Ocean; Prog. Oceanogr. 51,1–123.

Shcherbinin, A.D., Arsen'Yev, V.S., Gol'din, Y.A., 1979. The western boundary current of the Bay of Bengal (English translation). Dokl. Acad. Sci. USSR Earth Sci. Sect. 244, 167–168.

Shetye, S. R., Gouveia,A. D., Shankar,D., Shenoi, S. S. C., Vinayachandran,P. N., Sundar, D., Michael,G. S., Nampoothiri, G., 1996. Hydrography and circulation in the western Bay of Bengal during the northeast monsoon, J. Geophys. Res., 101(C6), 14,011–14,025.

Shetye, S. R., Gouveia,A. D., Shenoi,S. S. C., Michael,G. S., Sundar,D., Almeida,A. M., Santanam, K., 1991. The coastal current of western India during the northeast monsoon, Deep-Sea Res. Part A, 38(12), 1517–1529.

Sharma, R., Agarwal, N., Momin, I.M., Basu, S., Agarwal, V.K., 2010.Simulated Sea Surface Salinity Variability in the Tropical Indian Ocean. J. Clim. 23, 6542–6554. doi:10.1175/2010JCLI3721.

Sheng, J., Greatbatch, R.J., Zhai, X., Tang, L., 2005. A new two-way nesting technique for ocean modeling based on the smoothed semi-prognostic method. Ocean Dyn. 55, 162–177.

Stevens, D.P., 1991. The open boundary conditions in the United Kingdom fineresolutionantarctic model. J. Phys. Oceanogr. 21, 1491–1494.

Sindhu, B., Suresh,I., Unnikrishnan,A. S., Bhatkar,N. V., Neetu, S., Michael., G. S., 2007. Improved bathymetric data sets for the shallow water regions in the Indian Ocean, J. Earth Syst. Sci., 116, 261 – 274, doi:10.1007/s12040-007-0025-3.

Szekely, T., Gourrion, J., Pouliquen, S., and Reverdin, G.: The CORA 5.2 dataset for global in situ temperature and salinity measurements: data description and validation, Ocean Sci., 15, 1601–1614, https://doi.org/10.5194/os-15-1601-2019, 2019.

Treguier, A., Barnier, M., De Miranda, A.P., Molines, J.M., Grima, N., Imbard, M., Madec, G., Messager, C., 2001. An eddy permitting model of the Atlantic circulation: evaluating open boundary conditions. J. Geophys. Res. 106 (C10), 22115–22130.

Varkey, M.J., Murty, V.S.N. and Suryanarayana, A., 1996. Physical Oceanography of the Bay of Bengal and Andaman Sea, Oceanography and Marine Biology: anAnnual Review (eds A.D. Ansell, R.N. Gibson and Margaret Barnes), 34: 1-70.

Verezemskaya, P., Barnier, B., Gulev, S. K., Gladyshev, S., Molines, J.-M., Gladyshev, V., et al. 2021. Assessing eddying (1/12°) ocean reanalysis GLORYS12 using the 14-yr instrumental record from 59.5°N section in the Atlantic. Journal of Geophysical Research: Oceans, 126, e2020JC016317. https://doi.org/10.1029/2020JC016317

Vinayachandran, P.N.,Yamagata, T., 1998. Monsoon Response of the Sea around Sri Lanka: Generation of Thermal Domesand Anticyclonic Vortices. J Phys Oceanogr. 28. 1946-1960. 10.1175/1520-0485(1998)028<1946:MROTSA>2.0.CO;2.

1166 Vinayachandran, P. N., Kurian, J., 2007. Hydrographic observations and model simulation of
1167 the Bay of Bengal freshwater plume.Deep-Sea Res. Part I, 54(4), 471–486, doi:10.1016/
1168 j.dsr.2007.01.007.
1169 Vinayachandran, P. N.,Masumoto,Y., Mikawa,T., Yamagata,T., 1999.Intrusion of the
1170 Southwest Monsoon Current into the Bay of Bengal, J. Geophys. Res., 104(C5), 11077–
1171 11085, doi:10.1029/1999JC900035.
1172 Vinayachandran, P. N., Kagimoto, T., Masumoto,Y., Chauhan,P., Nayak, S. R., Yamagata,
1173 T., 2005.Bifurcation of the East India Coastal Current east of Sri Lanka.Geophys. Res.
1174 Lett., 32, L15606, doi:10.1029/ 2005GL022864.
1175 Vinayachandran, P. N.,Masumoto,Y., Mikawa,T., Yamagata,T., 1999.Intrusion of the
1176 Southwest Monsoon Current into the Bay of Bengal, J. Geophys. Res., 104(C5), 11077–
1177 11085, doi:10.1029/1999JC900035.
1178 Vinayachandran, P.N., Shankar,D., Vernekar,S., Sandeep,K.K., Amol,P., Neema,C.P.,
1179 Chatterjee, A., 2013.A summer monsoon pump to keep the Bay of Bengal
1180 salty. *Geophys.Res.Lett.,* 40:1,777–1,782, https://doi.org/10.1002/grl.50274.
1181 Vialard, J., Delecluse, P., 1998. An OGCM Study for the TOGA Decade. Part I: Role of
1182 Salinity in the Physics of the Western Pacific Fresh Pool. J. Phys.Oceanogr., 28, 1071 -
1183 1088.
1184 Valsala V**.,**Ikeda,M., 2007. Pathways and effects of the Indonesian Throughflow water in the
1185 Indian Ocean using Particle trajectory and Tracers in an OGCM. J. Clim, 20, 2994-3017.
1186 Webber, B. G. M., Matthews, A. J., Vinayachandran, P. N., Neema, C. P., Sanchez-Franks, A.,
1187 Vijith, V., Amol, P., & Baranowski, D. B. (2018). The Dynamics of the Southwest
1188 Monsoon Current in 2016 from High-Resolution In Situ Observations and
1189 Models, Journal of Phys. Oceanogr., 48(10), 2259-2282.
1190 https://journals.ametsoc.org/view/journals/phoc/48/10/jpo-d-17-0215.1.xml
1191 Wijffels, S. E., 2001. Ocean transport of freshwater, in Ocean Circulation and Climate, edited
1192 by G. Siedler, J. Church, and J. Gould, pp. 475– 488, Elsevier, New York.
1193 Wijesekera, H. W., Jensen,T. G., Jarosz, E., Teague,W. J., Metzger,E. J., Wang,D. W.,
1194 Jinadasa,S. U. P., Arulananthan, K., Centurioni,L. R., Fernando, H. J. S., 2015.Southern
1195 Bay of Bengal currents and salinity intrusions during the northeast monsoon, J.
1196 Geophys. Res. Oceans, 120, 6897–6913, doi:10.1002/ 2015JC010744.

Wijesekera, H. W., Teague, W. J., Wang, D. W., Jarosz, E., Jensen, T. G., Jinadasa, S. U. P., Fernando, H. J. S., Hallock, Z. R., 2016. Low-Frequency Currents from Deep Moorings in the Southern Bay of Bengal, J.Phys. Oceanogr.,, 46(10), 3209-3238. https://journals.ametsoc.org/view/journals/phoc/46/10/jpo-d-16-0113.1.xml

Wakelin, S.L., Holt, J.T., Proctor, R., 2009. The influence of initial conditions and open boundary conditions on shelf circulation in a 3D ocean-shelf model of the North East Atlantic. Ocean Dynamics 59, 67–81. https://doi.org/10.1007/s10236-008-0164-3

Zhou, Q., Mu, M., Duan, W., 2019. The initial condition errors occurring in the Indian Ocean temperature that cause "spring predictability barrier" for El Niño in the Pacific Ocean. J. of Geophy, Res,: Oceans, 124, 1244–1261. https://doi.org/10.1029/ 2018JC014403

Zuo, H., Balmaseda, M. A., Tietsche, S., Mogensen, K., Mayer, M., 2019. The ECMWF operational ensemble reanalysis-analysis system for ocean and sea-ice: a description of the system and assessment, Ocean Sci. Discuss., https://doi.org/10.5194/os-2018-154,

Zuo, H., Balmaseda, M. A., de Boisseson, E., Hirahara, S., Chrust, M., De Rosnay, P., 2017. A generic ensemble generation scheme for data assimilation and ocean analysis. ECMWF Tech Memo., https://doi.org/10.21957/cub7mq0i4, 2017.

Report of the Mercator Ocean International Marine Data Assimilation Workshop Workshop held in Toulouse on 5 & 6 September 2018.
https://marine.copernicus.eu/sites/default/files/wp-content/uploads/2018/11/MOI_MDA-Report-FVR.pdf

	Winter(DJF)		Spring (MAM)		Summer(JJA)		Fall(SON)	
	Mean	STD	Mean	STD	Mean	STD	Mean	STD
0-200 m	12	114	72	109	-99	72	42	108
0-1000m	-3	150	114	135	-55	102	92	77
0-2000 m	34	118	61	92	7	66	27	79
Entire depth	4.0	35	5	31	-23	42	-17	35

Table 1.The upper ocean (0-200 m) seasonal mean salt transport and its standard deviation (in psu-m^3/s). Positive (negative) values indicate northward (southward) transport.

Figures

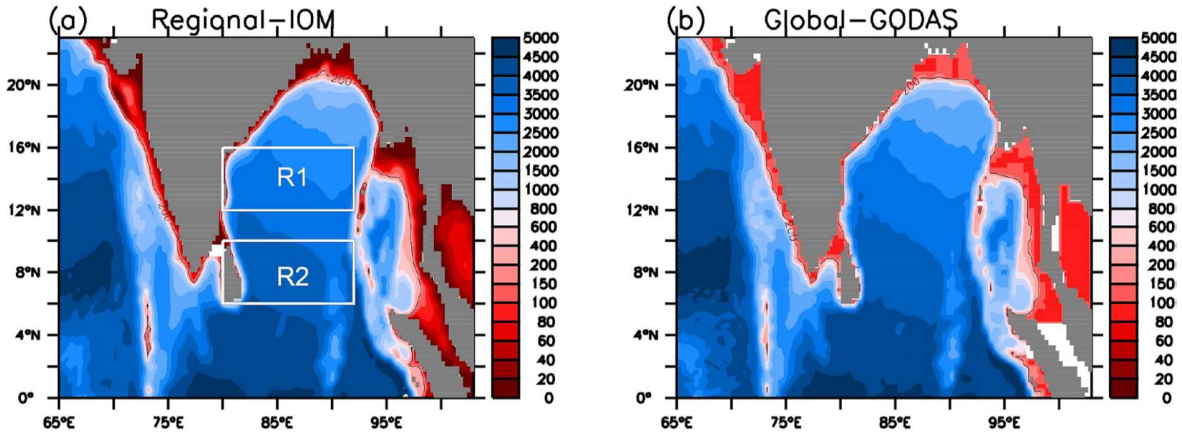

(c)

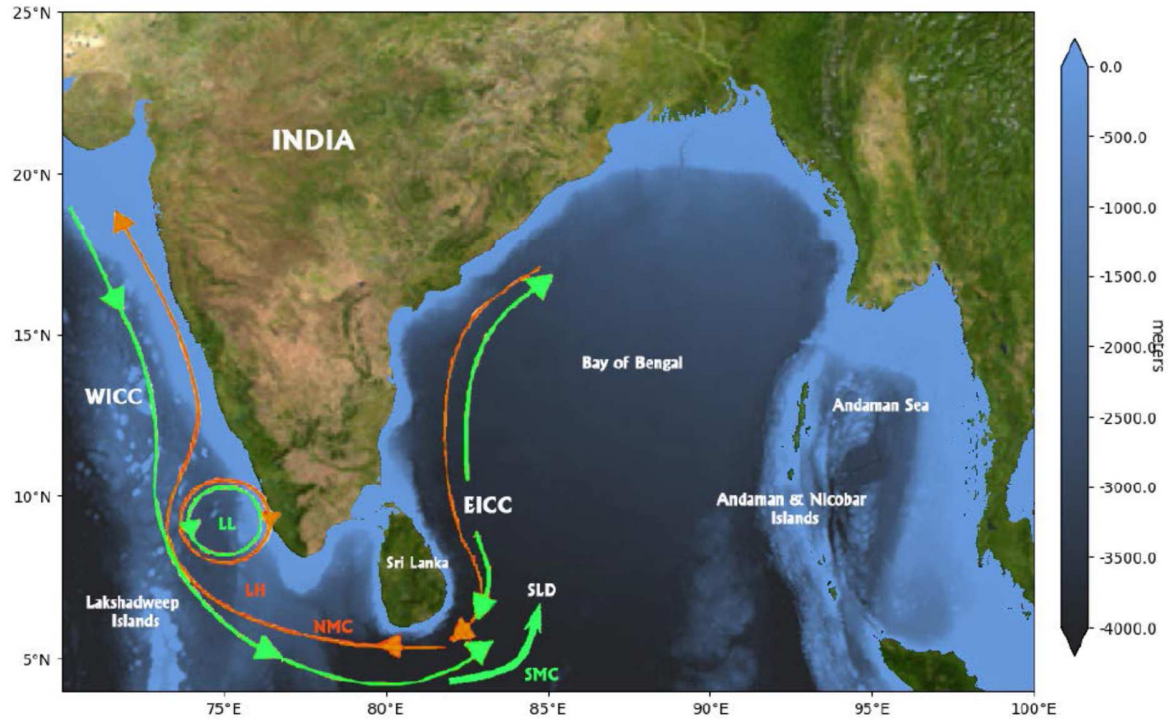

Figure 1.Bathymetry used in (a) regional simulations and (b) GODAS reanalysis. Notice the unrealistic water column depths in the coastal regions in the latter; (c) Schematic illustration of major currents along the Indian coast(green color for the summer season and orange for the winter season) – West India Coastal Current (WICC), Lakshadweep Low (LL), Lakshadweep High (LH), South-West Monsoon Current (SMC), North-East Monsoon Current (NMC), SLD (Sri Lanka Dome) and East India Coastal Current (EICC). WICC and EICC occur in both monsoons but differ in direction as indicated by the colored arrows.

Schematic adapted from Figure 1 of Bharti et al.(2021). The boxes (R1-Central Bay of Bengal : 80-92° E, 12-16°N ; R2- Southern Bay of Bengal-80-92° E, 6-10 °N) given in figure 1a are used to generate figure 8 and 9.

(a) **(b)**

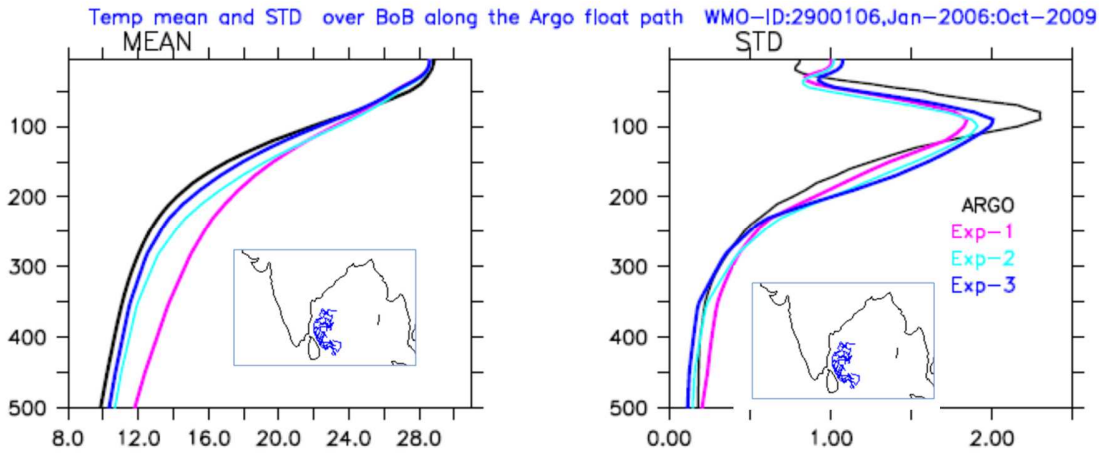

(c) **(d)**

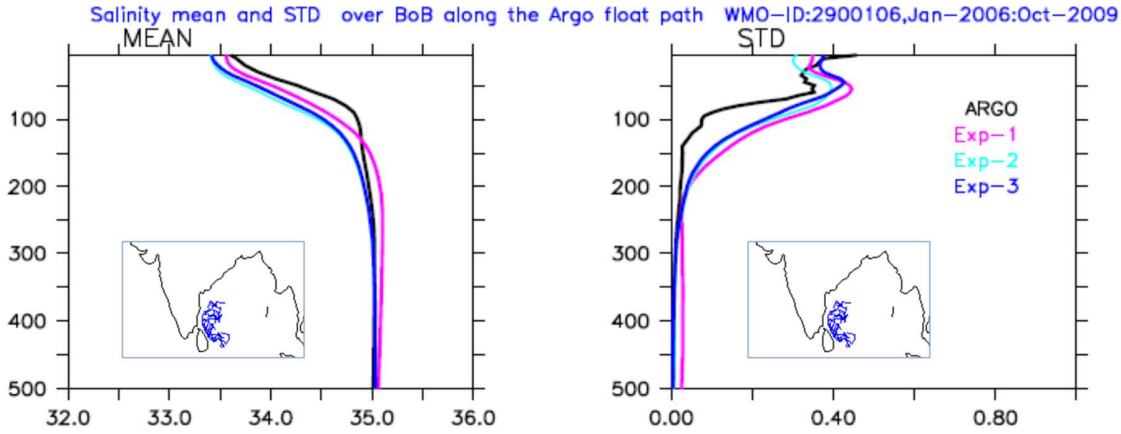

Figure 2. Model simulated temperature comparison with co-located and concurrent Argo profiling float observations over BoB: (a) Mean and (b) Standard Deviation for 2006-2009. Model simulated salinity comparison with collocated and concurrent Argo profiling float observations over the south Bay of Bengal: (c) Mean and (d) Standard Deviation for 2006-2009. The trajectory of the float is shown in the insets.

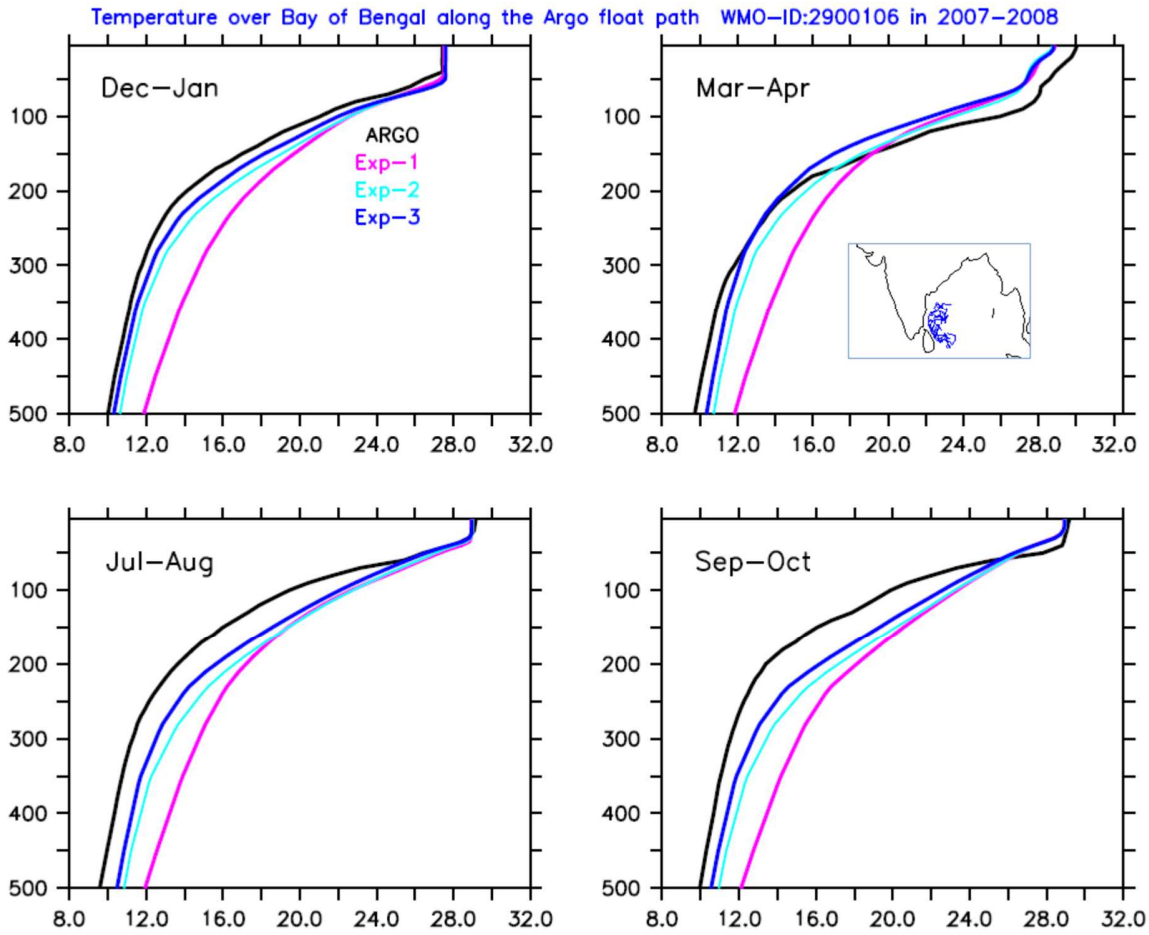

Figure 3.Comparison of seasonal model-simulated temperature with the co-located and concurrent Argo profiling float observation over southern BoB for 2007-2008. The trajectory of the float is shown in the inset of upper right hand panel.

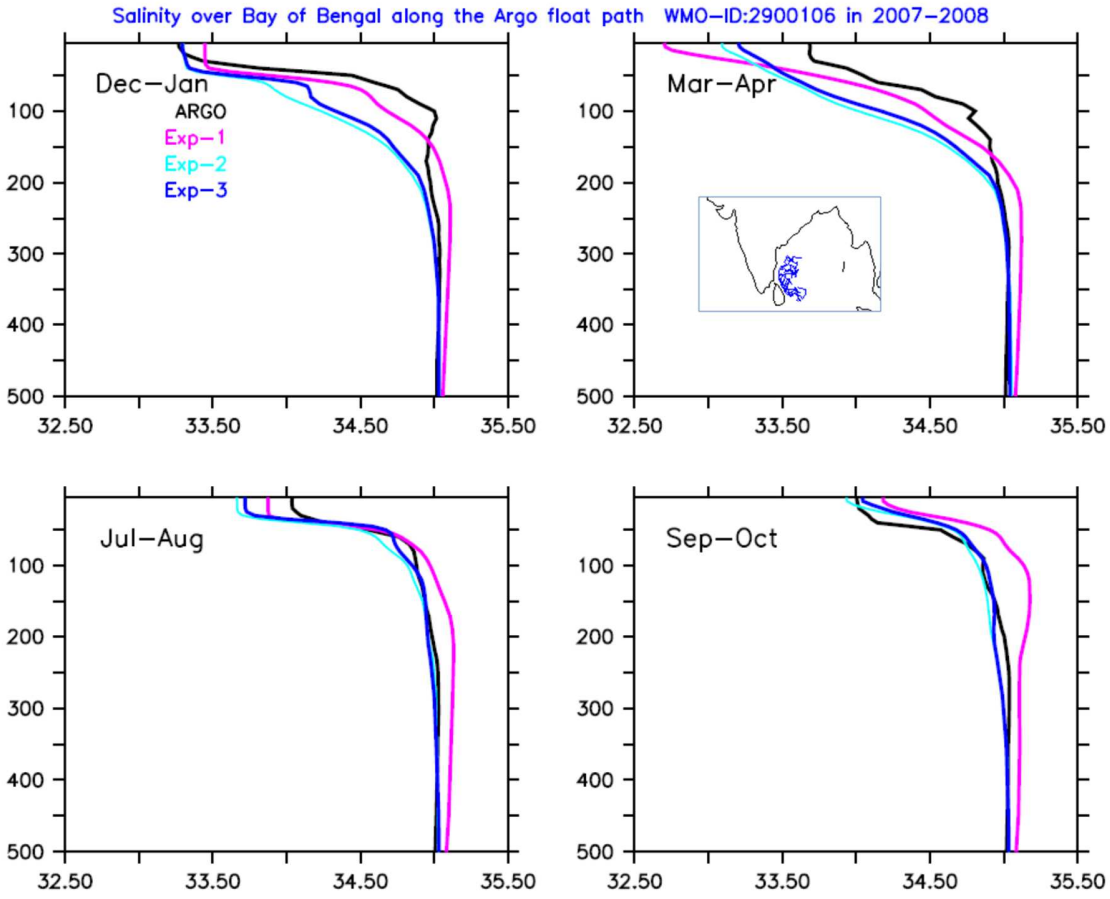

Figure 4. As in Figure 3, but for salinity.

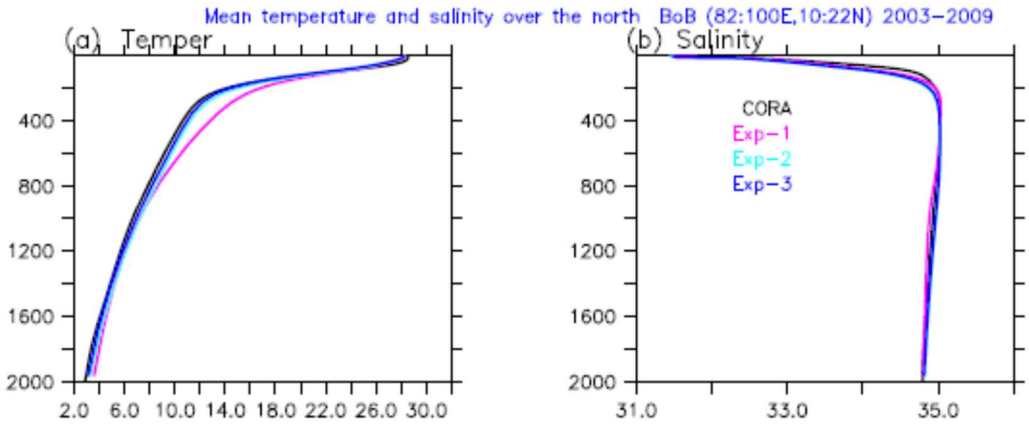

1290

1291 Figure 5.Comparison of model simulated mean temperature and salinity for 2003-2009 from
1292 the three experiments with gridded observation (CORA5.2) over northern BoB: (a)
1293 temperature and (b) Salinity.

1294

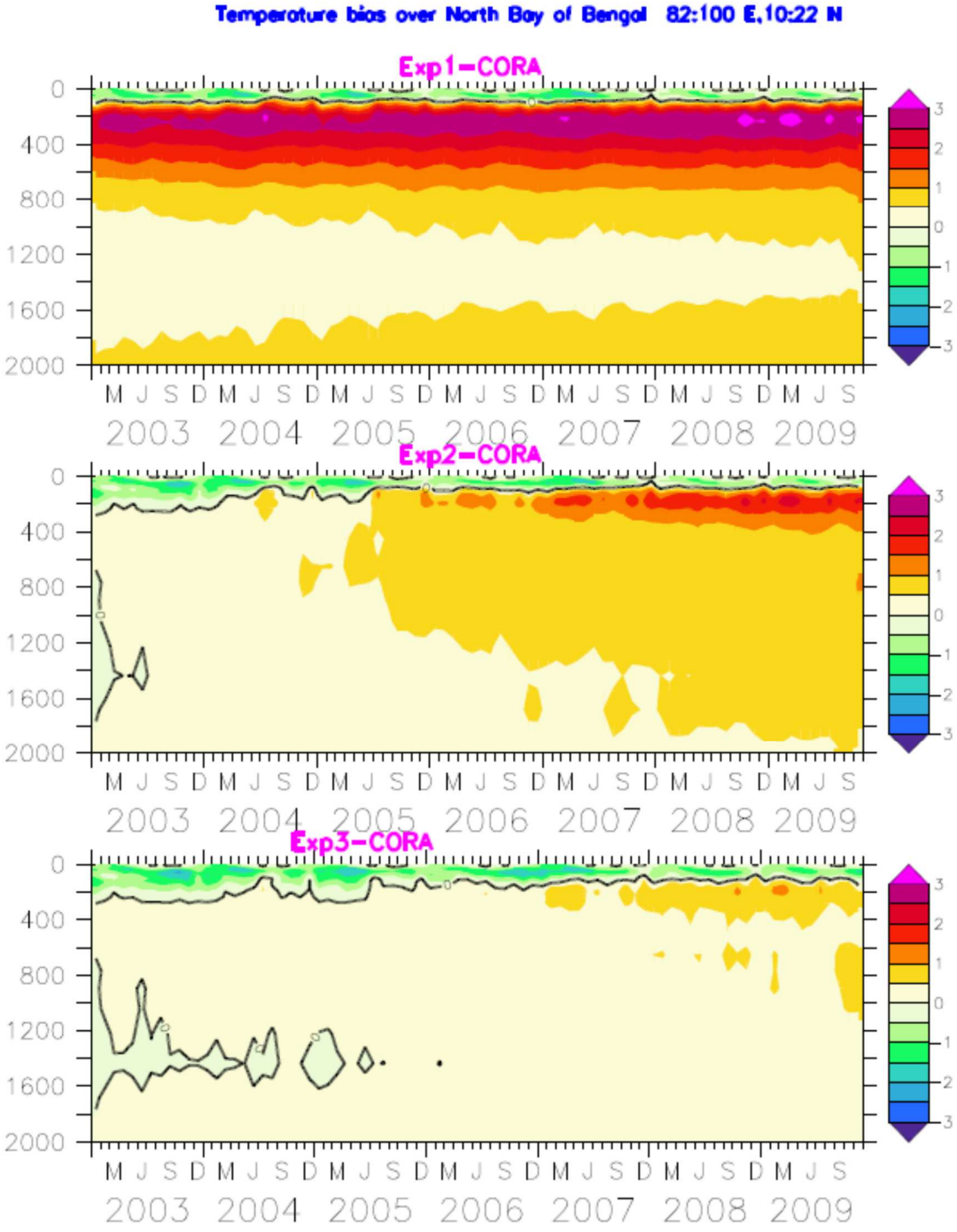

1295

1296 Figure 6**.** Depth vs time plots of the differences in temperature between the three simulations

1297 (Exp-1, -2, -3) and the observed gridded temperature over northern BoB.

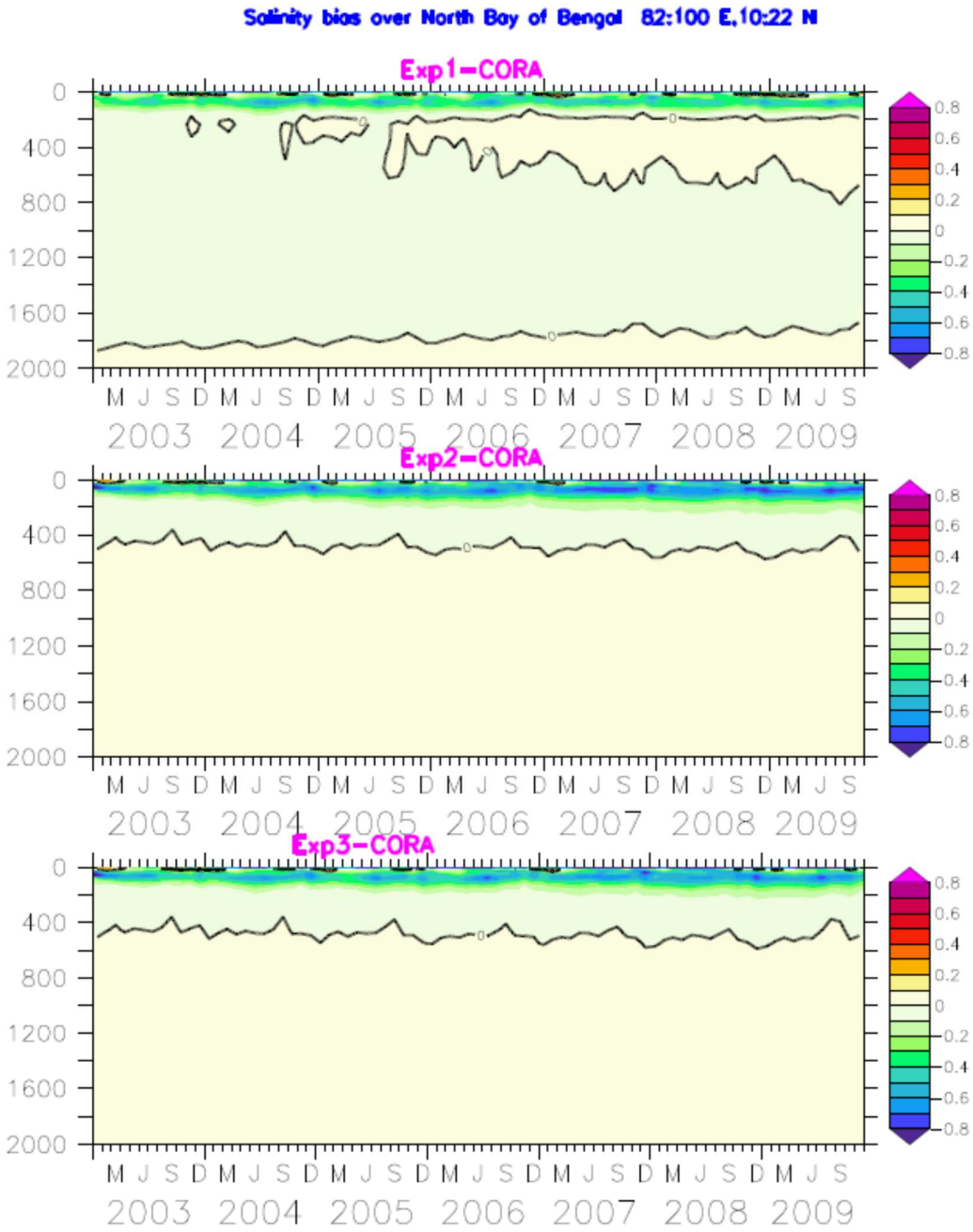

Figure 7. As in Figure 6, but for salinity.

(a)

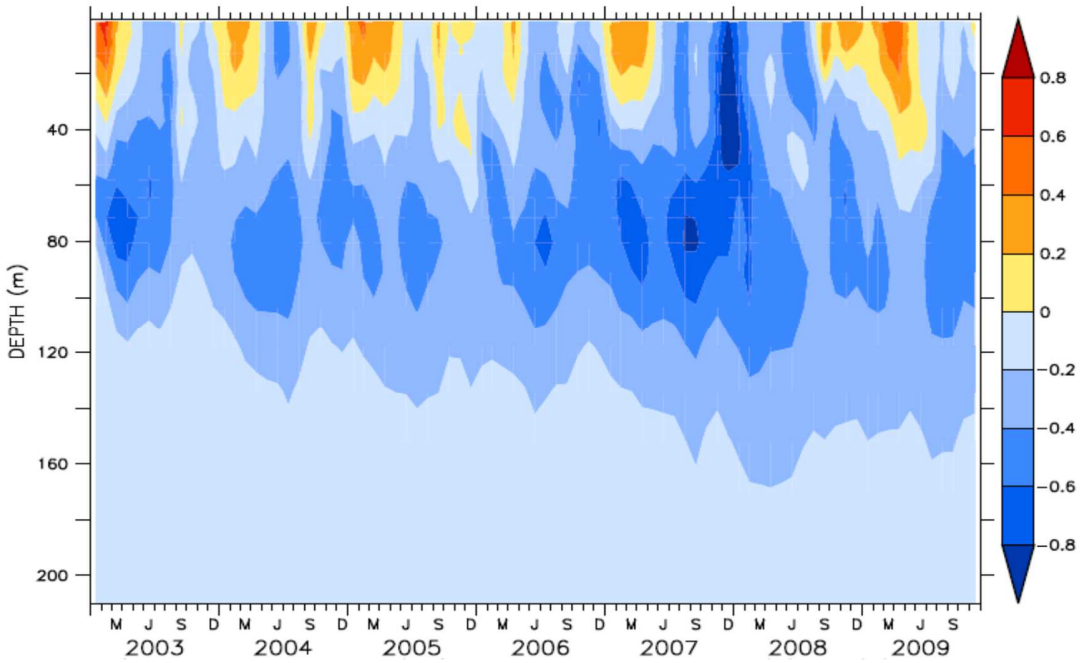

(b)

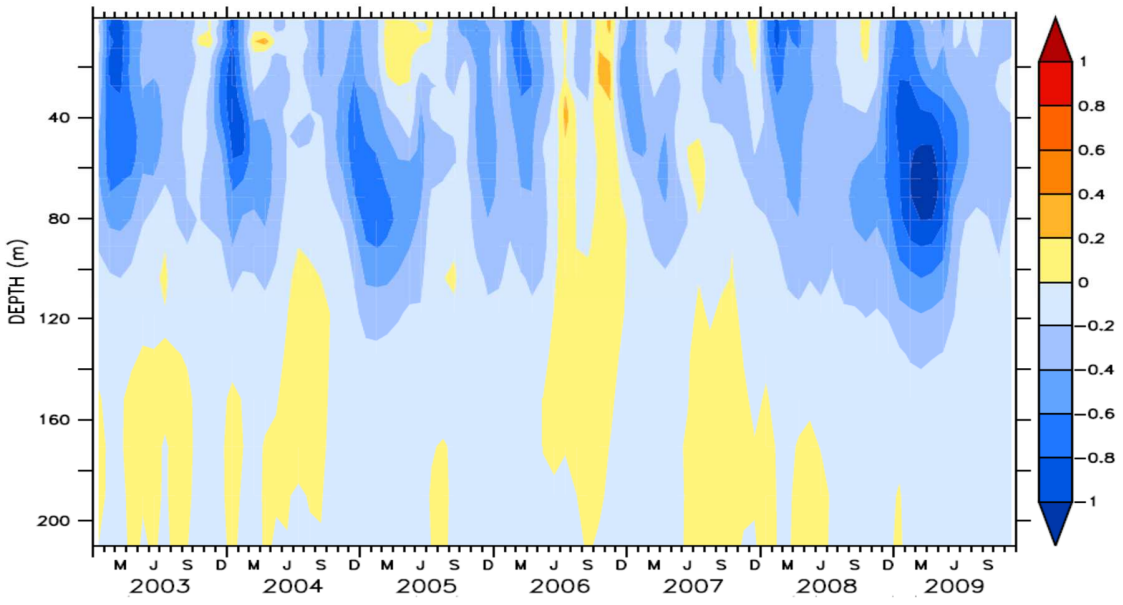

Figure 8. Depth vs. time plots of salinity bias in Exp-3 with respect to gridded observations (CORA5.2) averaged over 80-92 ° E in the upper ocean over BoB: (a) 12-16 °N, (b) 6-10 °N. (see the regions given as R1 and R2 for (a) and (b) in Figure 1a).

.

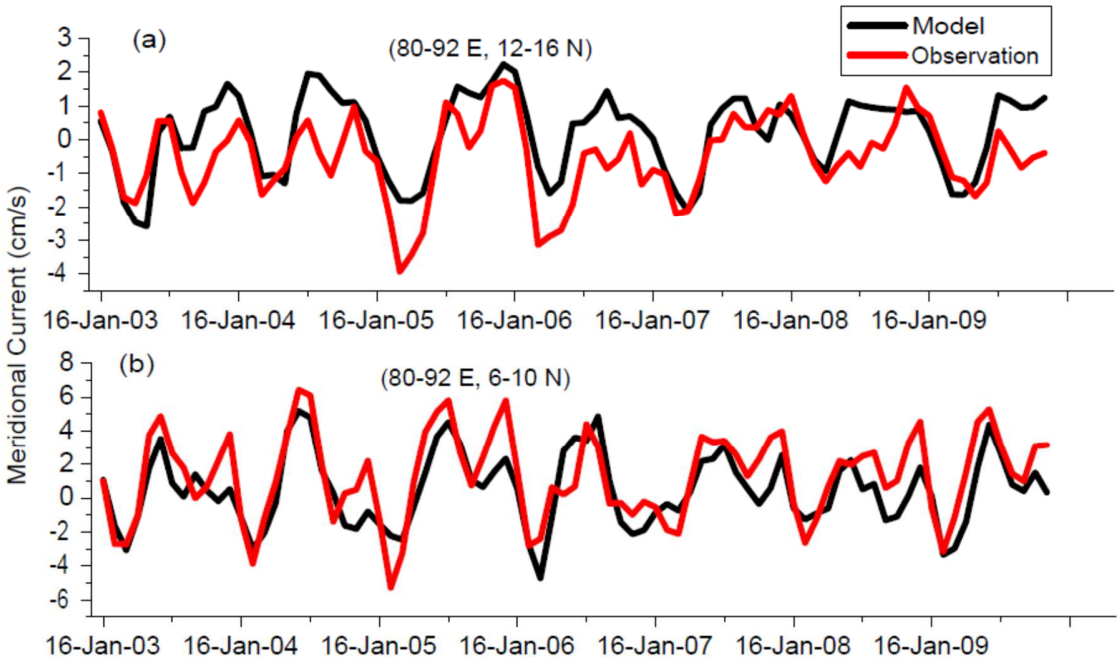

Figure 9. Geostrophic Currents (100 - 500 m) computed from Exp-3 model simulation compared to those from observed ORCA5.2 temperature and salinity fields over (a) Central BoB and (b) Southern BoB (see the regions given as R1 and R2 for (a) and (b) in Figure 1a).

.

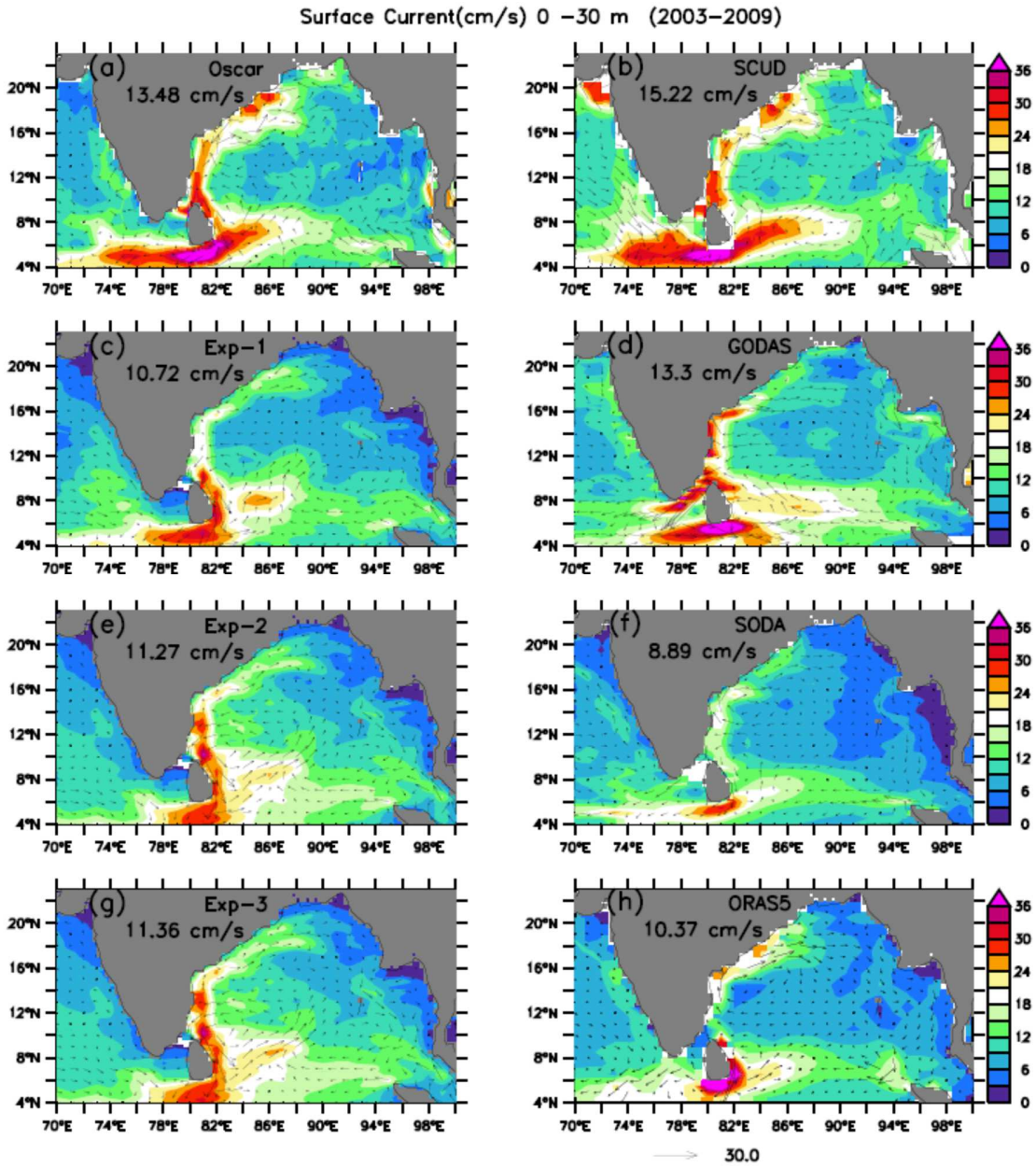

1321

1322 Figure 10. Model-simulated upper ocean (0-30 m) currents compared with OSCAR, SCUD,
1323 GODAS, SODA and ORAS5 for 2003-2009. The basin averaged current speeds (m/s) are
1324 shown in each panel.

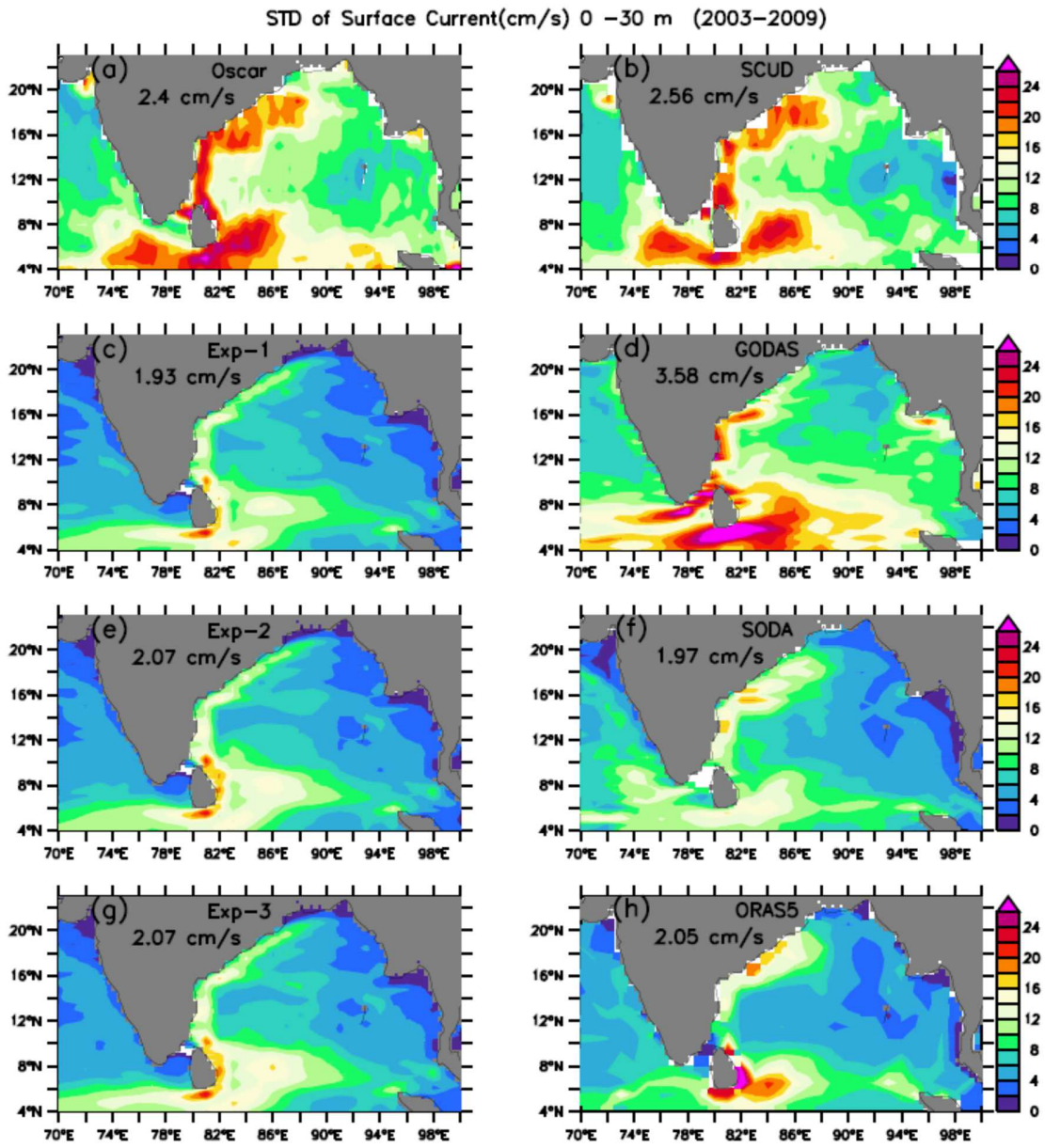

Figure 11: STD of model simulated upper ocean (0-30 m) currents compared with STD of OSCAR,SCUD, GODAS, SODA and ORAS5 values for 2003-2009. The basin averaged STD values (m/s) are shown in each panel.

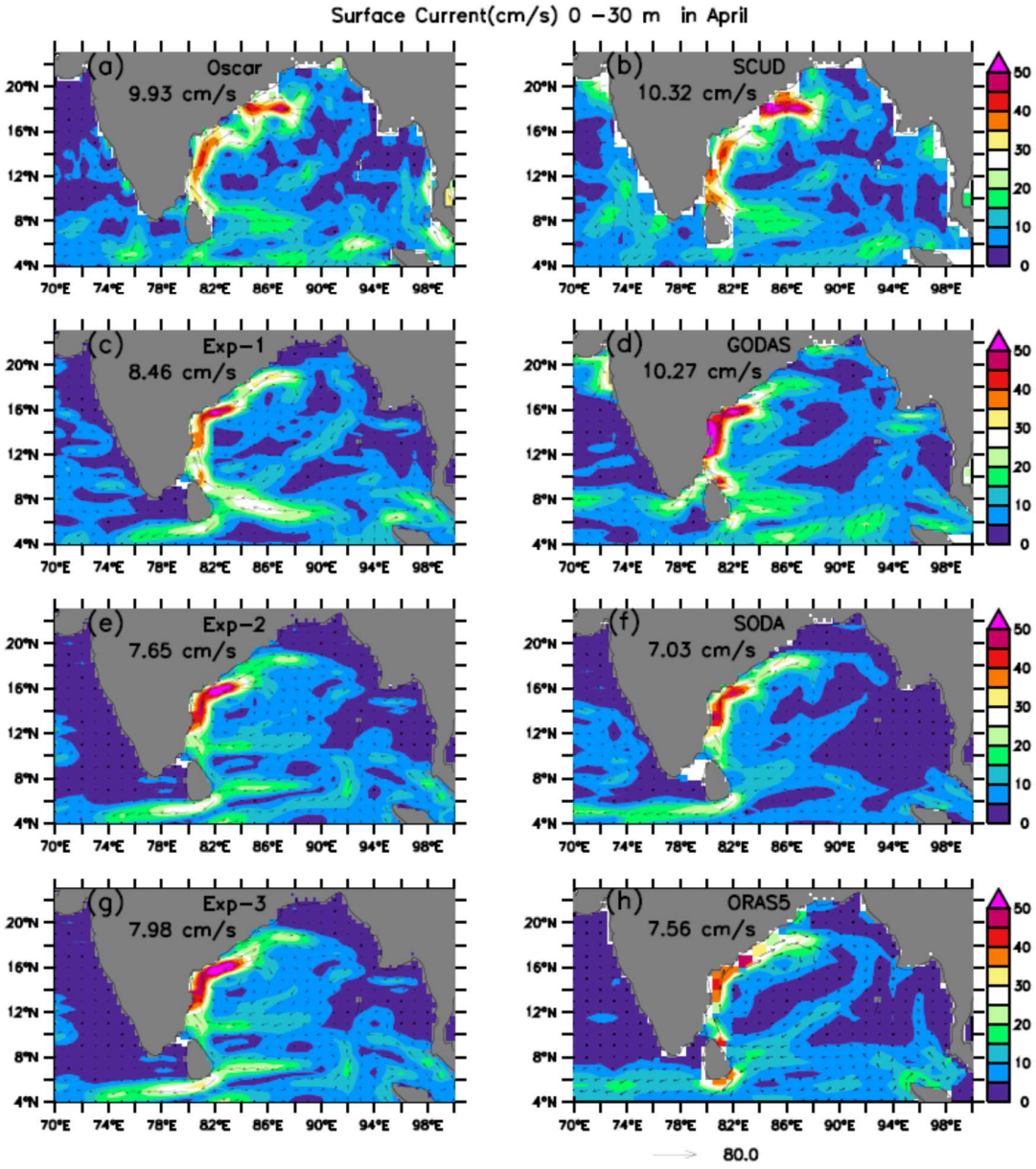

1330

1331 Figure 12.As in Figure 10, but for 2003-2009 April climatology.

1332

1333

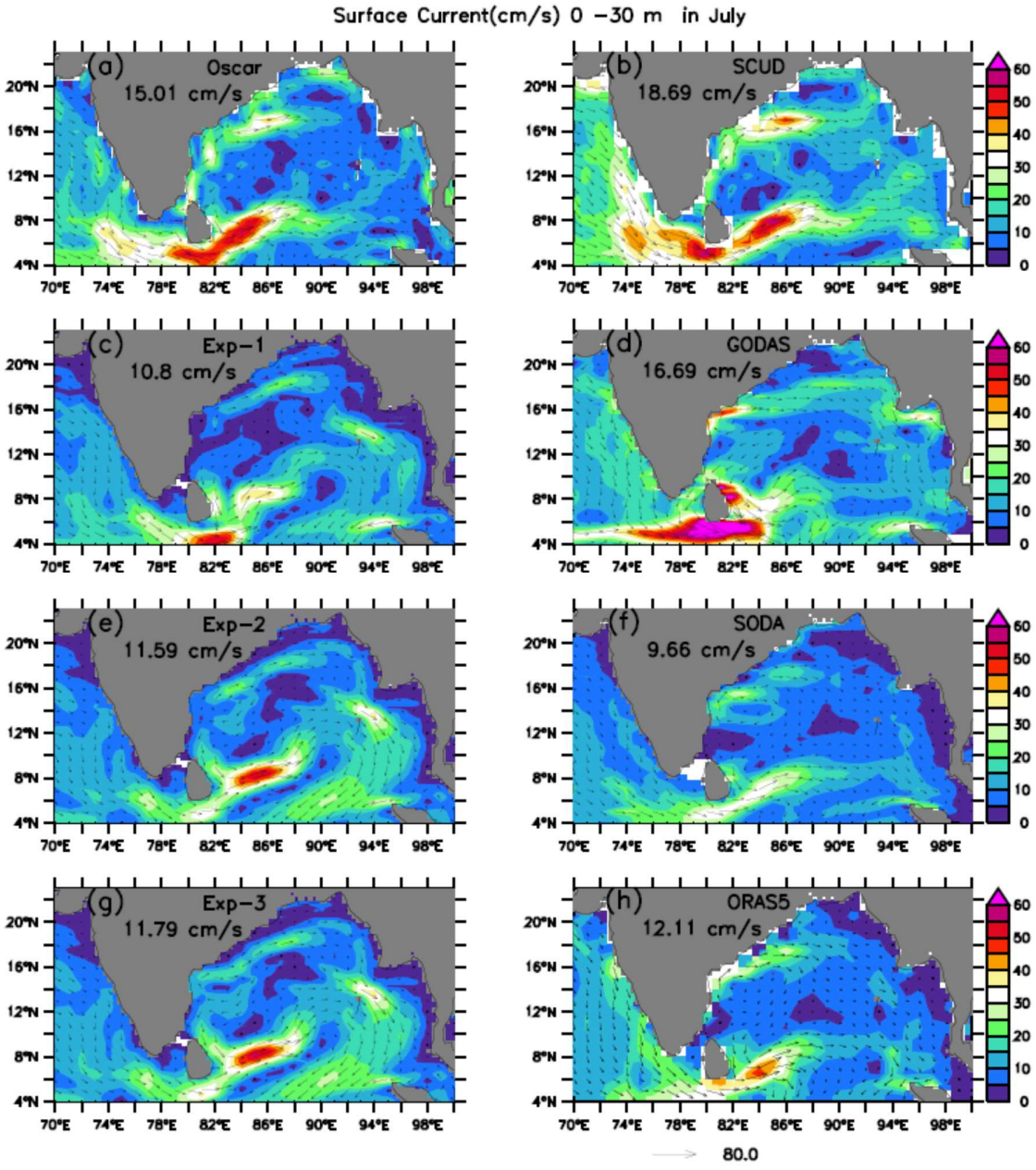

Figure 13.As in Figure 10, but for 2003-2009 July climatology.

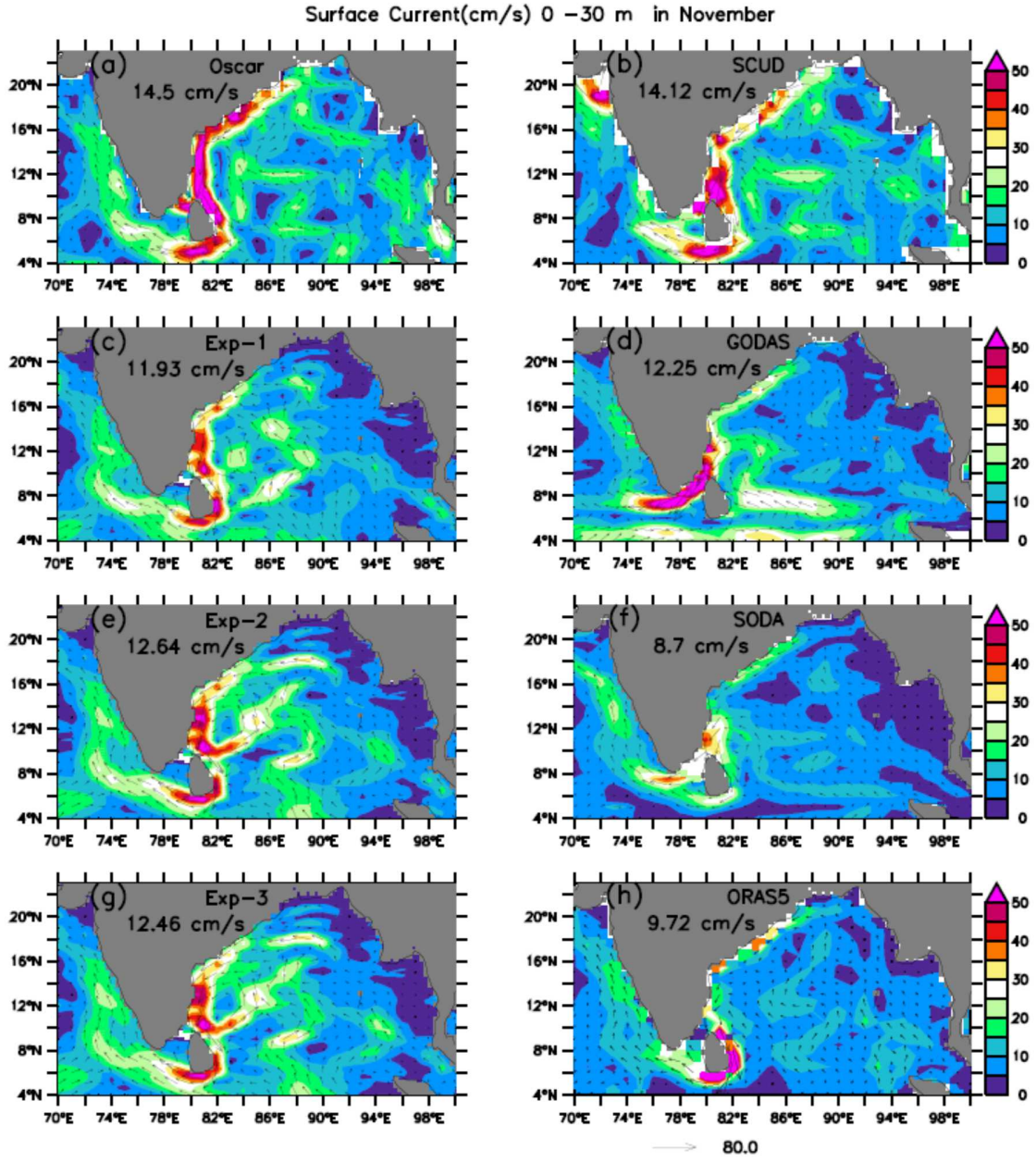

Figure 14.As in Figure 10, but for 2003-2009 November climatology.

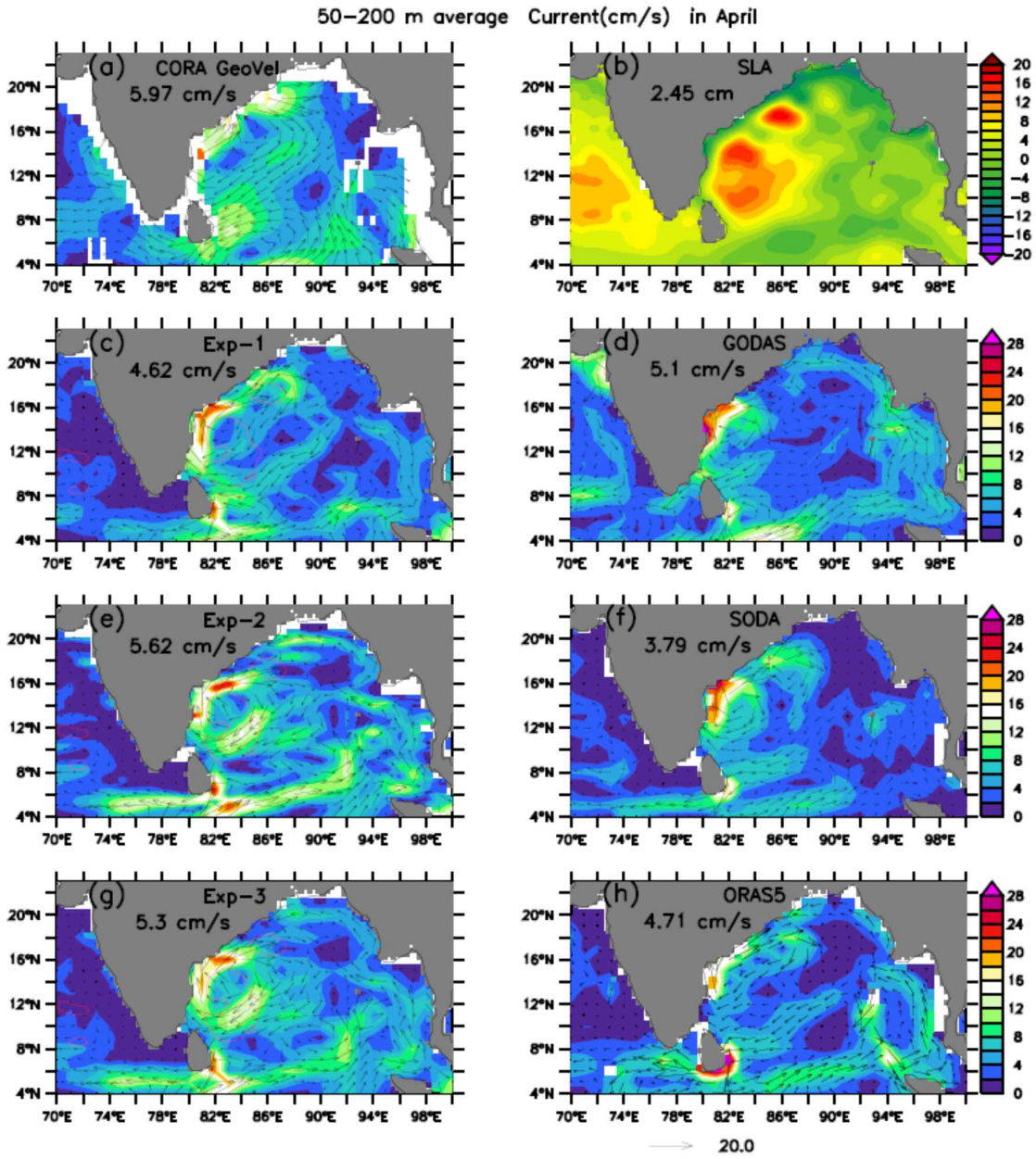

Figure 15. (a) April Geostrophic current climatology (2003-2009) computed with CORA 5.2 gridded temperature and salinity data. (b) Sea level anomaly from AVISO observation. Model-simulated thermocline (50-200 m) currents for 2003-2009 April climatology in BoB from Exp-1 (c), Exp-2 (e) and Exp-3 (g), GODAS (d), SODA (f) and ORAS5 (h) values. The basin-averaged mean values (m/s) are shown in each panel. The red contours in panels c,e and g are SLA also shown in panel (b).

1350

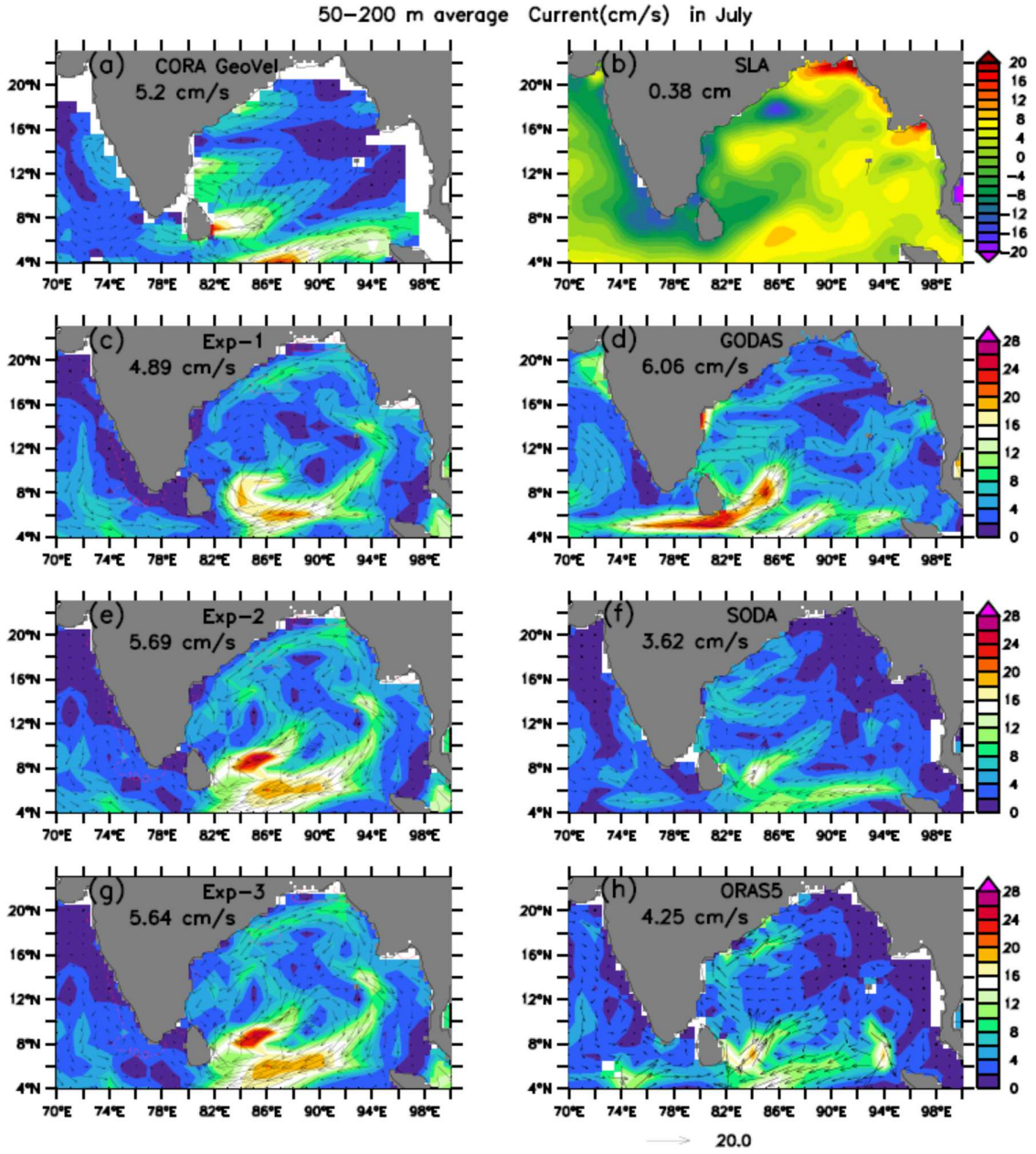

1351

1352 Figure 16.As in Figure 15, but for July climatology

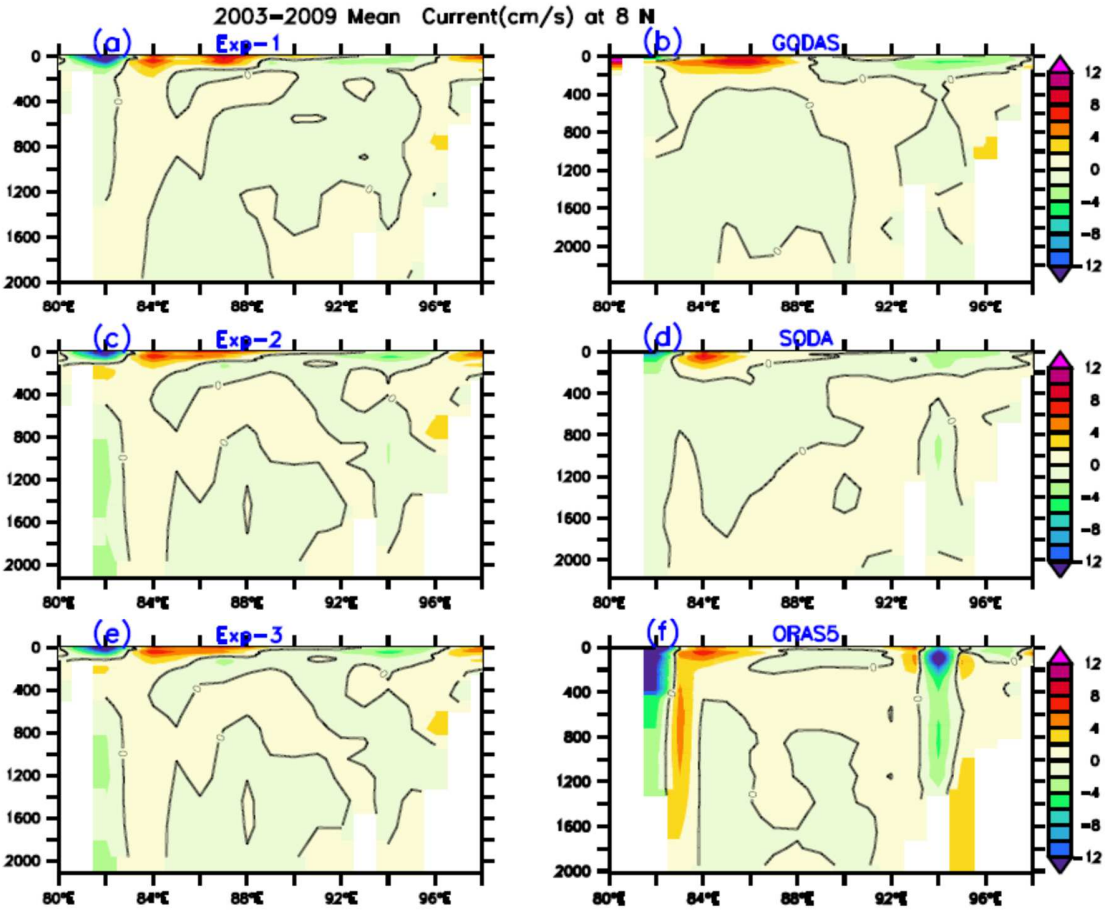

1353

1354 Figure 17. Mean meridional current along 8 ^{o}N for 2003-2009,from Exp-1 (a),Exp -2 (c) ,Exp

1355 -3 (e) and GODAS (b) ,SODA3 (d) and ORAS5 (f).

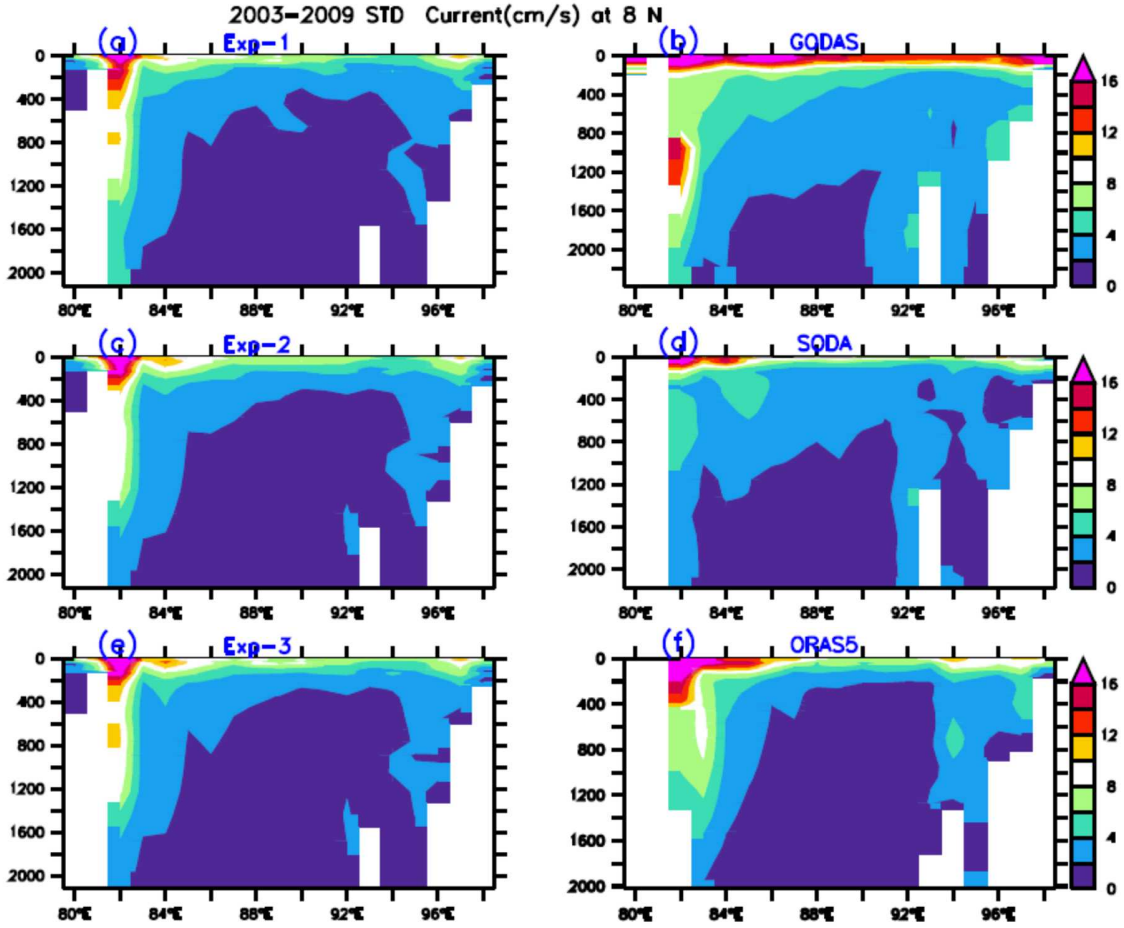

Figure 18.As in Figure 17, but for STD of meridional currents.

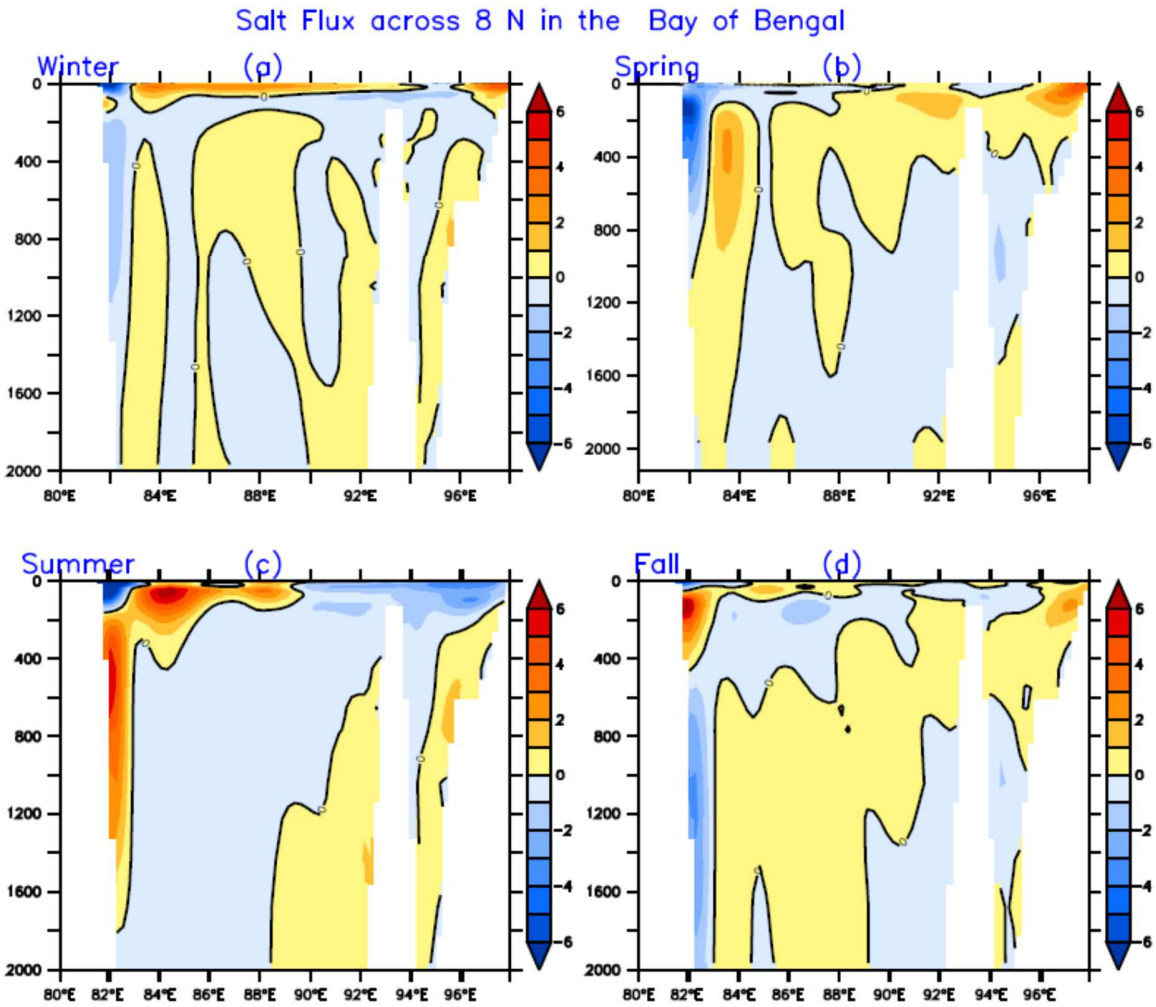

Figure 19. Seasonal mean salt flux (psu-m/s) along 8 °N for 2003-2009 in: (a) Winter, (b) Spring, (c) Summer, and (d) Fall.

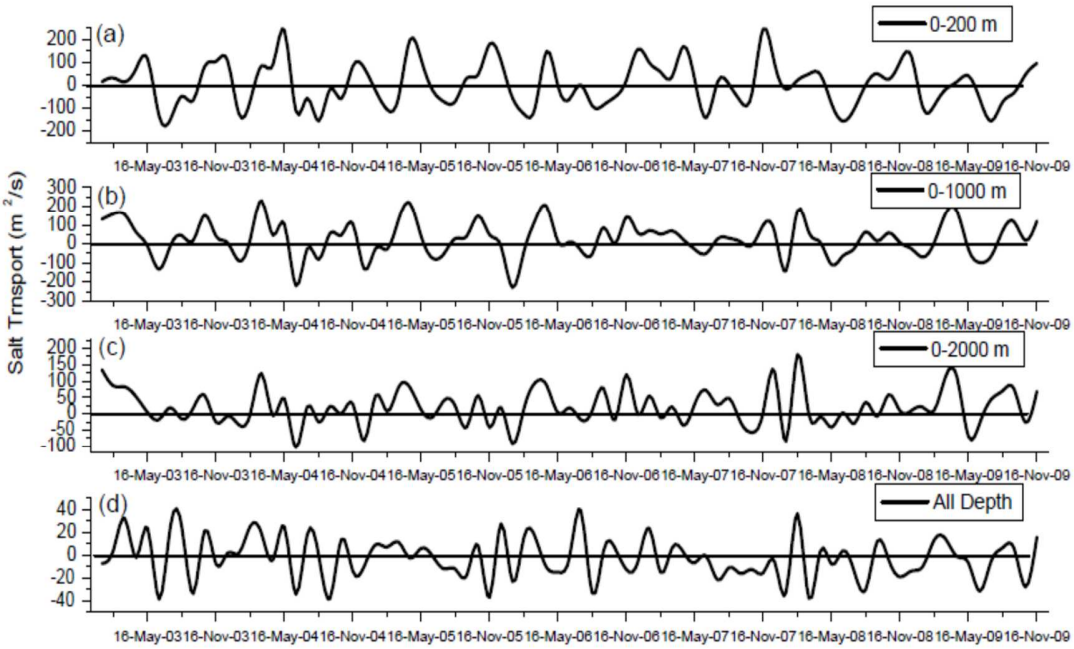

1364

1365

1366 Figure 20. Time series of depth-integrated seasonal salt transport (in psu-m^3/s) along 8 °N

1367 for2003-2009: (a) 0-200 m , (b) 0-1000 m (c) 0- 2000 m and, (d) all depth .

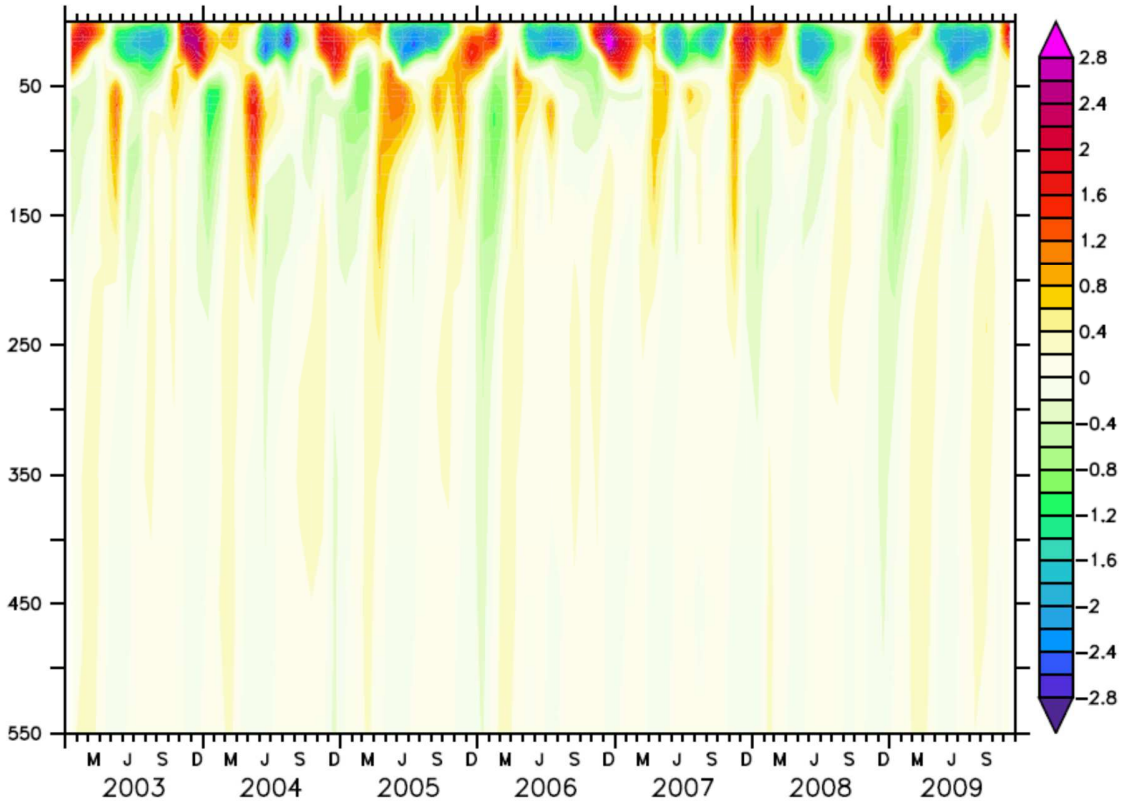

Figure 21: Depth vs. time Hovmollar plot of salt transport (in psu-m/s) along 8 ^{o}N.